Volume photoinscription of glasses: three-dimensional micro- and nanostructuring with ultrashort laser pulses

Razvan Stoian

Appl. Phys. A manuscript No.
(will be inserted by the editor)

Volume photoinscription of glasses: three-dimensional micro and nanostructuring with ultrashort laser pulses

Razvan Stoian

Received: date / Accepted: date

Abstract Ultrafast laser photoinscription of optical materials has seen a strong development in the recent years for a range of applications in integrated photonics. Fueled by its capability to confine energy in micro-domains of arbitrary geometries, it forecasts extensive potential in optical design. The process can locally modify the material structure and the electronic properties, changing in turn the refractive index. It thus lays down a powerful concept for three-dimensional modifications with the potential to design integrated optical functions. Using fused silica as model glass, this report discusses the physical mechanisms of photoinscription, outlining the possibility of refractive index engineering. We will review basic mechanisms of light propagation, excitation of matter, and energy relaxation concurring to material structural and photo-physical modification. A dynamic perspective will be given, indicating relevant times for relaxing different forms of energy (electronic, thermal, etc.). The possibility to structure beyond diffraction limit will be explored, as well as the subsequent optical response of hybrid micro-nano structures. Different irradiation geometries for photoinscription will be presented, pinpointing their potential to generate optical and photonic systems in 3D. Spatio-temporal pulse engineering can optimize the material response towards the achievement of accurate positive and negative index changes. An optimality concept can thus be defined for index design. A particular potential derives from the utilisation of non-diffractive beams with engineered dispersion. Finally we indicate a range of application domains, from telecom to optofluidics and astrophotonics, outlining the potential of volume micro and nanoprocessing.

Keywords Ultrashort laser pulses · material processing · glass · laser photoinscription · refractive index engineering · 3D photonics

R. Stoian
Laboratoire Hubert Curien, UMR 5516 CNRS, Université de Lyon, Université Jean Monnet, 42000 Saint Etienne, France
E-mail: razvan.stoian@univ-st-etienne.fr

1 Introduction

Nowadays advances in micro and nano-technologies depend on the development of processing tools able to structure materials in two- and three-dimensions with utmost precision and reduced collateral damage. Remote control with the capability to interface and drive process parameters becomes an essential advantage. An intensively studied and utilized processing method, with an employment field ranging from macroscale applications in cutting, drilling or welding to precise patterning in UV microelectronic lithography, relies on laser radiation. A more recent extension towards higher precision derives from the utilization of ultrashort fs (10^{-15} s) or ps (10^{-12} s) laser pulses [1]. Ultrashort laser processing has recently developed into a high performance technology able to take up novel processing challenges, with intrinsic structuring capabilities well into the nanoscale [2]. This relies on unmatched abilities to process materials using nonlinear excitation and limited thermal diffusion, generating high-end applications where energy localization by ultrashort pulses is critical. This impacts specifically the present attempts of miniaturization and packaging of several functions on a single support. A prominent example is the field of photonics and its importance in processing and transmitting information. The concept of a photonic chip integrating several optical functions in a single monolithic device is therefore crucial for the development of applications, and its performance can be dramatically facilitated by a three-dimensional design within an optical material.

The idea of three-dimensional modifications of transparent materials (glassy and crystalline materials with a forbidden gap significantly higher than the photon energy) as a driver of photonic integration is intrinsically related to the utilization of ultrashort pulses at a wavelength for which the material itself is transparent [3]. This allows to transport laser radiation at the impact point in the volume without losses and, via focusing, to concentrate the energy only at the region where the material has to be modified. The concentration of energy allows for the achievement of high intensities (in the range of TW/cm^2) only in a limited region approximately given by the confocal distance of the focusing element, these being capable of locally ionizing the material, modifying its structure and hence the local optical properties. A confined change of the refractive index occurs. This elementary unit for assembling an optical function can, via the positioning of the beam, be geometrically reproduced in three dimensions, outpacing thus standard capabilities used in planar technologies. This offers then a reliable and qualitatively pertinent processing method for fabricating optical elements and functions inside a material, with a capability to transport and manipulate light in three dimensions. The present photolithographic methods (sometimes accompanied by ion exchange), though, highly precise for surface and near surface processing, are hard to extrapolate in three dimensions and require a layer by layer approach. The multistep procedure renders the process expensive and complex. Therefore, due to their non-contact approach, ultrashort laser pulses make design and integration of multiple functions in three dimensions feasible and simpler. On the longer

term, they will permit optical integration with mass production batch methods and digitalized processes.

Since the first demonstration of volume refractive index modifications in transparent materials for optical guiding using ultrashort laser pulses in the mid-nineties by Davis *et al.* [4], the field of 3D ultrafast laser photoinscription experienced a significant development. This breakthrough advancement was preceded or accompanied by attempts to modify bulk materials by catastrophic damage or by color center generation [5,6]. In the light of the importance of understanding and evaluating optical damage for optical components, the interest has led laser application since the early times, at the same time with attempts towards understanding the mechanisms of photosensitivity [7–11]. Photosensitivity has equally led to the early development of optical sensors based on optical Bragg resonances [12,13]. The use of ultrashort pulse has then brought specific challenges for focusing in the bulk and a certain resistance to damage [14] for reasons that will be discussed later, putting forward solutions involving tight focusing and dispersion control. The concept of three-dimensional modifications has recently evolved towards the nanoscale, based on an enhanced capability of ultrashort laser pulses to create upon focusing regions of high intensity on extreme spatial scales that can go beyond the diffraction limit. These harness efficiently the absorption nonlinearity and drive new paths of material modifications. If ultrafast laser photoinscription can confine energy in micro-scale domains of arbitrary geometries, modifying the material refractive index and, at the same time, laying down the concept of 3D design for efficient optical functions, nanoscale precision can deliver high levels of performance. Therefore bypassing the diffraction limit is key for a new range of applications in optics and mechanics requiring optical access to the nanoscale. Exploiting the nonlinearity of excitation, ultrashort laser pulses show remarkable capacity to localize light on subwavelength scales, building up on collective carrier effects on surfaces and in the bulk. Control of laser interaction by beam design can drive selected physical paths and geometries and we focus here on structural evolutions in the bulk outlining dimensional scales enabled by spatio-temporal beam shaping [15].

The purpose of this article is to briefly review the concept of ultrashort laser pulse design of refractive index and give a perspective on its potential for fabricating embedded optical elements and functions into the mass of an optical material. The discussion is structured in several parts. First we will briefly review general aspects of the interaction of ultrashort pulses with dielectric materials. A detailed analysis can be found in Ref. [16]. We will present physical mechanisms concurring to the material transformation upon the laser impact, indicating the possible ways of controlling refractive index changes. Fused silica is used as a model material for photoinscription studies. We will give in addition a brief description of the behavior of other transparent materials. We then follow the dynamics of electronic excitation in confinement conditions and point out characteristic times of energy deposition, serving as guidelines for control. We will explore the influence of pulse temporal and spatial design in achieving index structures on scales approaching 100 nm, either

in direct focusing or in self-organization schemes. We will describe the most effective irradiation techniques to facilitate the optical design, together with their advantages and drawbacks. We equally discuss the capability of Gauss and Bessel-Gauss pulses with engineered dispersion to localize light on sub-wavelength scales. We show how sculpting beams in space and time can bring advantages for controlling the interaction between light and matter and for achieving extreme confinement of energy. The local refractive index change serves then as a building block for either generating elementary optical functions (guiding, filtering) or for enabling complex passive and active optical processes. We describe the fabrication of waveguides, polarizing or filtering devices and give examples of complex high-performance embedded optical systems for current applications in information transmission, data communication, sensing, optofluidics, astrophotonics and quantum optics. We underline photonic systems where hybrid micro/nanoscale features can develop advanced optical functionalities.

2 Physical mechanisms of photoinscription

2.1 Ultrashort laser pulses

The physical and chemical transformation of matter upon irradiation is the consequence of the energy deposition from the laser pulse to the material, intermediated by electrons. It comprises a series of events related to excitation, energy relaxation, and modification of matter. The processes occur on multiples spatial scales covering molecular, mesoscopic and macroscopic domains. They follow a dynamic evolution with characteristic times specific to the relaxation path. The challenge of high processing resolution is defined by the need to confine the deposited energy at the frontiers of optical limits. To this, one needs to impede energy diffusion by achieving matter transformation rapidly, on extreme timescales, hence, by the use of ultrashort laser pulses (fs and ps range). An insightful description of the generation and the characteristics of ultrashort pulses was recently given in Ref. [17] (and the references within). An ultrashort laser pulse is essentially a wavepacket of light (field $\mathcal{E}(t), \tilde{\mathcal{E}}(\omega)$ described in temporal and spectral domains respectively) oscillating at a specified carrier frequency ω_0, being mathematically described as a Fourier decomposition of monochromatic waves $\mathcal{E}(t) = 1/2\pi \int_{-\infty}^{+\infty} \tilde{\mathcal{E}}(\omega) e^{i\omega t} d\omega$. The pulse duration is inversely proportional to its spectral bandwidth. The shortest pulse for a given spectrum can be obtained when the individual spectral components are synchronized so that they can arrive in the same time at the same point. Their relative retardation is zero. However, if the composing frequencies travel with a variable relative retardance $\varphi(\omega)$ (a different relative phase for each spectral component), expressed as $\tilde{\mathcal{E}}(\omega) = |\tilde{\mathcal{E}}(\omega)| e^{i\varphi(\omega)}$, this will impact their relative temporal delay expressed by a temporal phase redefining the field as $\mathcal{E}(t) = |\mathcal{E}(t)| e^{-i\Phi(t)}$ [17]. This puts forward the challenge of controlling the dispersion of the pulse in order to harness all the advantages

related to a short energy packet. The essential impact of ultrashort laser pulses in material processing is firstly related to the speed of energy deposition into the electronic system, before significant transfer to the molecular matrix, with the subsequent light-driven non-equilibrium between electrons and phonons, and, secondly, to the achievable intensities in the TW/cm^2 range, beyond the limit for material destruction. Their action directly on atomic and molecular dynamics scale, before significant heat generation and diffusion occurs, favors interaction which is commonly coined as athermal, with a strong nonlinear character.

The typical durations delivered by commercial lasers designed for industrial applications are in the 100 fs–10 ps range for wavelengths in the near infrared, 800 nm for the Ti:Sapphire technology or 1030 nm for the diode pumped Yb-based amplification media to only give few examples. Focusing this type of radiation at the diffraction limit ($\sim \lambda/2$ for the highest numerical apertures currently available) i.e. on a sub-micron dimension can generate extremely high intensities at levels enough to ionize all materials, as their electronic structure would be strongly altered in the presence of a high intense field. The field strength (of tens and hundreds of GV/m) becomes here comparable to the material binding strength. To harness all benefits for industrial applications, the process should be controllable and this is based on a thorough understanding of the interaction process. We discuss below the physical mechanisms leading to well-defined material modifications and notably to a refractive index change in optical transparent materials. These will cover aspects of excitation, nonlinear propagation and physical paths of energy relaxation and material modifications. We will highlight different regimes of light-matter interaction, from linear effects at low intensities, perturbative regimes with the onset of $\chi^{(2)}$ and $\chi^{(3)}$ nonlinearities to effects characteristic to the strong field regimes.

2.2 Nonlinear excitation

The material support of interest for three dimensional refractive index engineering is in most cases a dielectric material, usually glasses or crystals presenting a large forbidden energy gap E_{gap}. Polymers are also of interest as cost-effective materials. Notwithstanding also interest in semiconductor materials (e.g. Si photonics) or narrow gap glasses for mid-infrared applications, we will concentrate on large band-gap materials as the main characteristics can be extrapolatable to other gap materials. Mostly fused silica will be considered as a model case.

The process of laser ionization and energy deposition can be easily understood using the electronic structure of the solid [18]. The transparent materials present an occupied valence band build by superposition of molecular orbitals of the constituents (for example O and Si orbitals for a silica glass) and a free conduction band, separated by an interval of several eV (7-9 eV in case of fused silica). The material is normally transparent at the irradiation wavelength (typically in near infrared). This property enables the transport of light

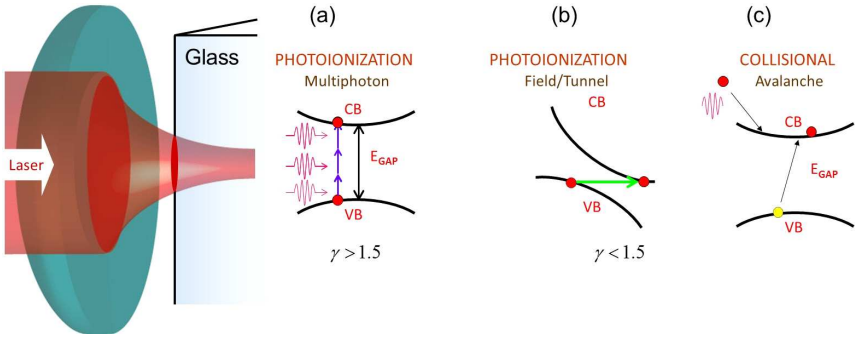

Fig. 1 Schematic representation of ultrafast laser ionization processes. (a) Multiphoton ionization across a large band-gap. (b) Tunnel ionization in strong fields. (c) Collisional ionization and carrier multiplication.

into the bulk, as the photon energy is too small (e.g. 1-3 eV) to promote electrons over the forbidden energy gap by single absorption events. This observation is valid for low intensities. The presence of an intense laser field modifies the electronic band structure and occupation allowing thus to deliver energy to the electronic system and then to the material. This photon-mediated interaction is called photoionization, referring to the ability to excite electrons via the laser field. The process occurs via several phenomena, all triggered by the high intensity, highlighted in figure 1; multiphoton processes, field ionization, and collisional ionization. A comprehensive theory of electronic excitation processes was given by L. V. Keldysh [19]. We review here some of the basic linear and nonlinear physical processes that govern how ultrashort laser pulses behave in transparent material in material structuring regimes.

The multiphoton process (MPI): In spite of the material transparency, when the photon density is high, a nonlinear absorption process occurs with the simultaneous absorption of several photons of energy $h\nu$, enough to bridge the gap and generate free carriers that oscillate in the laser field (quiver). In this case the absorption order is given by the ratio of the energy gap and photon energy; $N = [E_{gap}/h\nu]+1$. The absorption yield depends on the probability of having N photons at the same time at the same place, and follows an I^N dependence (equivalent to the same power dependence of the photon rate density), with I being the intensity. The typical photoionization rate $\frac{\partial \rho_e(t)}{\partial t}\mid_{PI} = W_{PI}$ can be generically expressed as $W_{PI} = \sigma_N I^N$ (with σ_N being simply the multiphoton absorption cross-section, accounting at the same time for the density of absorbing centers and for the photon energy). For intensities in the vicinity of the damage threshold in fused silica the photoionization rate lays in the 10^{16} 1/fs cm^{-3} range [20]. The process is schematically depicted in Fig. 1(a), illustrating the absorption of multiple photons creating a population of free electrons with low kinetic energy (minimum energy being the oscillation energy in the optical field), oscillating at the bottom of the conduction band. The presence of field can equally impact the band structure and photocurrents

at high ponderomotive energy via e.g. dynamic Stark and Franz-Keldysh effect. Field effects lead to Zener and photon assisted tunneling [21,22]. It is worth noting that the presence of extrinsic absorption centers with localized levels within the gap (e.g. defects, dopants) will lower the multiphoton order. Similarly the use of smaller wavelengths will make MPI more efficient.

Field ionization; tunnel ionization (TI) and above barrier ionization (ABI): The process (Fig. 1(b)) is conceptually different from MPI and occurs for higher intensities and larger wavelengths. In this case the laser field can lower the Coulomb barrier that binds the electron to its parent atom. Consequently, there is a non-negligible probability for the electron to tunnel through this barrier in a continuum of free states before the field reverses sign, the probability being dependent on the height of the barrier (increasing with the decrease of the barrier height). This is called tunnel ionization. In the event that the barrier is completely suppressed by the strong laser field, the electron can freely escape to the continuum of free states in a process of above barrier ionization. In both processes the electron is set free in the conduction band without requiring the absorption of multiple quanta of energy. The transition between tunnel ionization and multiphoton ionization is expressed via a nondimensional parameter called Keldysh adiabatic parameter γ ($\gamma = \omega\sqrt{2m_e E_{gap}}/e\mathcal{E}$, with ω being the laser frequency, E_{gap} the bandgap energy, $\mathcal{E}$ the electric field, e, m_e the electronic charge and mass). This reflects the duration of the process (as the time required for the electron wavepacket to develops underbarrier components) with respect to the oscillation period of the field (a discussion about tunneling time and its meanings can be found in [23]). For $\gamma > 1.5$ multiphoton processes dominates, while tunnel ionization takes over for $\gamma < 1.5$, i.e. for high intensities or large wavelengths [24]. Laser processing applications take usually place around $\gamma \simeq 1.5$ suggesting a mix of multiphoton and tunneling ionization processes. A model based on Zener tunneling and avalanche was presented in [25]. The photoionization regime becomes thus critically dependent on the pulse duration and the spectral content of the laser pulse, with very short durations and large wavelengths favoring the field-induced effect rather the multiphoton processes. Nevertheless we are in a range where the laser radiation strongly influences via the associated ponderomotive potential the optical properties of the solid.

The collisional ionization (CI): Once electrons are brought into the conduction band they behave as free mobile electrons. The presence of the cycling field imparts already an oscillation energy to the mobile charge, and thus, cycle-averaged, a ponderomotive energy. Carrier oscillations are dephased by interaction with scattering centers. Through collisions they continue to absorb energy from the laser field via inverse Bremsstrahlung. The energy gain of the electron in the laser field is essentially related to the capacity to collide (optimally at every half cycle, as to realign with the field), with an overall change of the momentum. If the energetic electron acquires an energy superior to the gap $E_{el} > E_{gap}$ ($E_{el} > 1.5E_{gap}$ to properly fulfill the conservation laws)

by sequentially absorbing multiple quanta, it can collide and ionize (knock off) a second electron from the valence band across the gap, leading thus to two free electrons of smaller energy at the bottom of the conduction band (flux-doubling [26]). They will be further accelerated in the field and will produce a collisional exponential-like multiplication of the electronic population. In a simple perspective the electron generation rate $\frac{\partial \rho_e(t)}{\partial t} \mid_{CI} = W_{CI}$ can be expressed as: $W_{CI} = \beta \rho_e I$ with β being the avalanche coefficient. The collisional ionization term W_{CI} depends on the local intensity (for the energy gain) and on the number of seed electrons (collision partners ρ_e), and through β on the inverse Bremsstrahlung strength and the material bandgap. That implies the existence of seed electrons capable of being accelerated, which are typically produced by the laser front. The process is illustrated in Fig. 1(c) and can have a strong contribution if the collision time is smaller than the laser pulse, allowing for several collisions. The processes, similar to the inverse Bremsstrahlung absorption cross-section, is favored by larger wavelengths.

All these phenomena will contribute to the generation of an electron-hole plasma with the density ρ_e, with mobile electrons in the conduction band, and an equivalent population of holes, presumably less mobile in the valence band (see [27] for a review of electronic processes). This occurs according to the rate equation [26] (or a series of rate equations [28] to better capture intraband dynamics) that includes for simplicity only photoionization (multiphoton, tunneling), electron heating and collisional ionization, and assumes a non-depleted valence band. The decay term is here a generic term which may include various paths of decay via trapping or recombination and more complex dependencies on densities as several partners may contribute to the recombination process (e.g. Auger).

$$\frac{\partial \rho_e}{\partial t} = W_{PI} + W_{CI} - \frac{\rho_e}{t_{decay}} \tag{1}$$

The fact that seed electrons are produced by the ultrashort laser pulse itself from a valence band occupied with high spatial uniformity before being accelerated confers high reproducibility and a deterministic character, where the optical field tailors the absorption which does not rely on extrinsic factors (e.g. statistic distribution of prior defects, etc.) anymore [25]. In other words, the laser creates its own absorption centers to sustain efficient absorption. At strong ionization rates depletion of the band occurs and the source terms should be corrected with $(\rho_{VB} - \rho_e)/\rho_{VB}$ with ρ_{VB} being the total reservoir susceptible to be ionized.

With the generation of a plasma, the dielectric function changes and develops an imaginary term, with the solid becoming absorbing, and the refractive index complex $n = \Re[n] + i\Im[n]$. In a Drude formalism for an ensemble of non-correlated carriers, the variation of the refractive index $\Delta\tilde{n}$ becomes:

$$\Delta\tilde{n}_{Drude} = -\frac{\rho_e}{2n_0\rho_{cr}} \frac{1}{1 + i/\omega_0\tau} \tag{2}$$

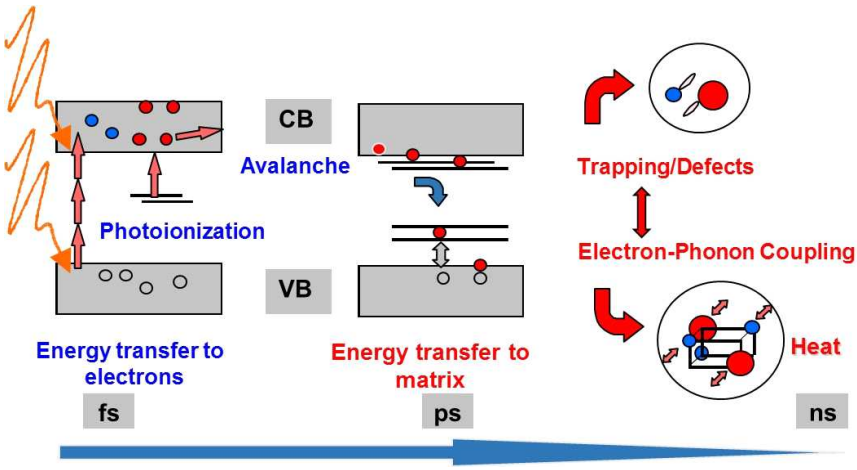

Fig. 2 Global view of excitation and relaxation processes in a dielectric material with relevant timescales. Photoexcitation processes and relaxation pathways are outlined [29].

with $\rho_{cr} = \epsilon_0 m_e \omega_0^2 / e^2$ being the critical density in vacuum, cancelling the real dielectric function (optical plasma resonance). m_e is the optical carrier mass (equal to the reduced effective mass of the electron and the hole) and τ is the momentum scattering time (see [18] for a discussion on carrier scattering models). This collision time reflects losses in the carrier response to the field and represents a way of transferring energy to the solid, provided that the collisions change the total momentum of the electron gas, defined by the Matthiessen rule (normally electron-ion/atom collisions and in certain limits electron-electron collisions). Besides field-induced ponderomotive effects, a net energy gain from the laser is therefore intrinsically related to a variation of the momentum, with these collisions constituting at the same time a leak of energy towards the collisions partners, the solid matrix, depending on their inelastic or elastic character.

For carrier densities above the critical value (ρ_{cr}), the initially transparent solid becomes absorptive and its refractive index decreases, with the response intermediated by electrons. The real part of the dielectric function goes negative and the transparent solid turns metallic in the focal region. As a function of the damping character or value (expressing the duration of τ with respect to the field period), the response becomes more or less abrupt, corresponding to collisional or less collisional plasmas.

At the same time the process deposits energy into the material with a loss term for electron generation given by:

$$\frac{\partial I(z,t)}{\partial z} = -W_{PI} N h\nu - aI(z,t) \tag{3}$$

with a being the absorption coefficient of the free carrier plasma ($a = 4\pi\Im[n]/\lambda$). The strength of inverse Bremsstrahlung determines the free electron heating and the efficiency of collisional multiplication. At the end an

electron-hole plasma is created that will intermediate the energy transfer to the molecular matrix, with a schematic presentation in Fig. 2 [29]. The matrix can gain energy to a certain extent during the electron-phonon interactions intermediated by a collision partner and massively after the light exposure has ceased, during the relaxation of the hot electrons. Models of plasma ionization are discussed in [26,30,31] based on rate equations and kinetic collisional theories. Complex quantum theories (i. e. Density Functional Theory) can be applied to observe the behavior of the excited solid [32]. Then, the energy transfer can occur on various timescales reflecting different channels, including mechanical, heat driven or non-thermal pathways. Continuum models and molecular dynamics can describe the solid transformation. Before discussing plasma relaxation paths via thermal and electronic channels, we should first be concerned with ways of preserving the intensity to the impact point. This relates to propagation issues during beam delivery and nonlinear pulse propagation becomes a key element [33]. The next section succinctly presents the potential factors of spatio-temporal beam distortions during delivery.

2.3 Linear propagation

In the linear regime the propagation of light in a material is governed by the Maxwell's equations. Upon propagation, the electric field determines inside the material a certain polarization by creating a dipole response of the free (not existing in a dielectric material) and bound electrons related to oscillating charge displacements in the field. Upon focusing via standard optical elements of finite numerical aperture, the spot is limited in size by diffraction [34]. In the case of a uniformly illuminated diffraction-limited optical system, the Airy spot at the focus has the radius at the zero intensity point $w_0 = 0.61\lambda/NA$, with λ being the wavelength and NA the numerical aperture. Correction factors can be applied for truncation ratios and pupil illumination patterns. The process is illustrated in Fig. 3(a) for uniform and Gaussian illumination.

In what concerns volume interactions, bulk processing of dielectrics involves typically crossing a planar air-dielectric interface. Taking into account the spectral bandwidth of an ultrashort laser pulse, the beam will suffer upon focusing a range of perturbations including spherical and chromatic aberrations. The wavefront is perturbed, affecting the capacity to focus. The result is an elongation of the modification trace with the focusing depth (Fig. 3(b,c)) that has to be accounted for in photoinscription strategies.

With the increase of intensity the material response depends nonlinearily on the strength of the applied optical field and the propagation becomes nonlinear [35]. Further complexity appears for resonant cases or for strong field regimes, when the optical field becomes comparable with the strength of the atomic field.

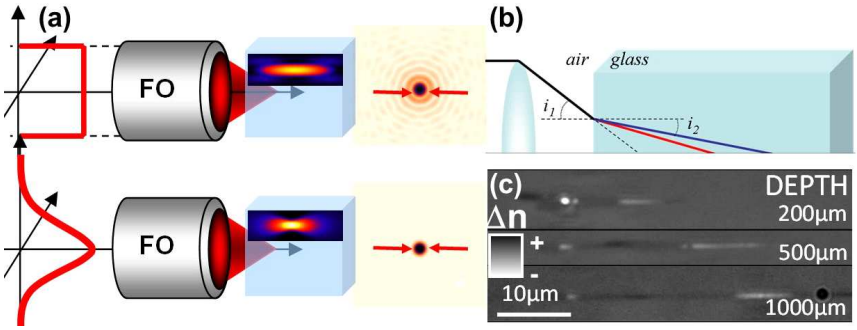

Fig. 3 Laser photoinscription concept for 3D processing. (a) Focusing using different pupil illumination techniques (uniform, Gaussian). (b) Aberrations upon focusing a light wavepacket of finite spectral bandwidth through an air-dielectric interface. (c) Typical damage traces as a function of the focusing depth underlining the longitudinal extension of damage with the depth.

2.4 Nonlinear propagation

A short laser pulse is inherently spectrally broad. The specific condition to harness all the intensity is to lock the composing spectral frequencies together. However, during focusing, the short laser pulse crosses a dielectric material that will exert in turn a strong influence on the pulse. Therefore a coupled action light-material will trigger several beam distortion phenomena in the spectral and temporal domain (see [33] for a review). In addition for intermediate intensities, smaller than the Coulomb field, the laser field becomes perturbative for the atomic states. Processes intermediated by nonlinear susceptibilities $\chi^{(2)}$, $\chi^{(3)}$ are determined by bound-bound transitions. Further increase in intensity determines ionization and a transition towards strong field regimes. An overview of potential nonlinear pulse distortion factors in the space and the time domain are schematically represented in Fig. 4.

Dispersion : The condition to have a synchronous interaction and interference of the frequencies that compose the pulse is to have a zero relative phase relation across the spectrum $\varphi(\omega) = 0$ (or constant). Developing the phase in a Taylor series, one obtains:

$$\varphi(\omega) = \varphi(\omega_0) + \varphi^{'}(\omega_0)(\omega - \omega_0) + \frac{1}{2}\varphi^{''}(\omega_0)(\omega - \omega_0)^2 + ... \qquad (4)$$

with $\varphi^j(\omega_0) = \frac{\partial^j \varphi(\omega)}{\partial \omega^j} \mid_{\omega_0}$ being the derivative of the order j. The first term is constant and has no effect while the second corresponds solely to a time translation of the pulse without affecting its time envelope. The higher terms will lead to a stretch and distortion in time of the frequency components, impacting the time envelope of the laser pulse as well as the arrival order of individual frequencies. The first derivative, the group delay describes the delay of the peak envelope. The second derivative, the group delay dispersion,

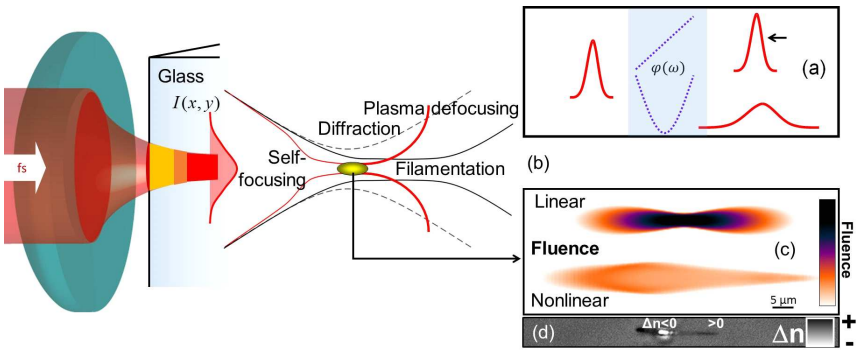

Fig. 4 Examples of linear and nonlinear propagation effects; (a) Dispersion and pulse stretching. (b) Kerr self-focusing and filamentation, (c) Calculated fluence distribution for a linear and nonlinear propagation case showing the limiting effects on energy deposition. (d) Measured refractive index trace in fused silica (phase contrast microscopy) with the catastrophic destruction of the material at the self-focusing point.

implying a quadratic phase dependence, indicates the broadening of the pulse as different frequencies travel at different velocities. This is related to a linear frequency sweep in the temporal domains, the so called chirp. The pulse will be elongated in time with either red or blue frequencies travelling first, with the accumulated phase depending on the material dispersion $n(\omega)$ (as illustrated in Fig. 4(a)). A review of the effect of dispersion terms on the pulse envelope is given in [17].

Self-focusing (SF): Whenever the intensity becomes high the effect on the material is strong and determines a significant polarization to accommodate the action of the laser field. The response of the material becomes nonlinear, and the polarization can be described as a power series of the field $\mathcal{P}(t) = \epsilon_0\chi^{(1)}\mathcal{E}(t) + \epsilon_0\chi^{(2)}\mathcal{E}(t)\mathcal{E}(t) + \epsilon_0\chi^{(3)}\mathcal{E}(t)\mathcal{E}(t)\mathcal{E}(t) + ...$ (valid for a lossless dispersionless medium with instantaneous response). Indeed, attosecond dynamics in the response time of the electronic polarization by a few-cycle laser pulse was recently measured [36], and, in general, delay times smaller than the laser period are expected, depending on intensity. Hence, given the intensity-dependent $\chi^{(3)}$, the refractive index will follow a similar behavior. As the intensity $I(r,t)$ depicts commonly a spatial and temporal dependence, it triggers thus spatial and temporal dependencies of the refractive index. For an isotropic medium such as glass, odd terms do not contribute due to inversion symmetry ($\mathcal{P}(t) = \epsilon_0\chi^{(1)}\mathcal{E}(t) + \epsilon_0\chi^{(3)}\mathcal{E}(t)\mathcal{E}(t)\mathcal{E}(t)$). The spatial part of the nonlinearity is at the base of a spectacular phenomenon; the self-focusing. For a Gaussian pulse, the nonlinear dependence $n(r) = n_0 + n_2 I(r)$ implies a maximization of the index at the center of the beam. A self-induced positive lens is created and the pulse will start to focus under its own action via Kerr lensing. Above a certain critical power ($P_{cr} = 3.77\lambda^2/8\pi n_0 n_2$ [37]), the Kerr focusing will overcome the natural diffraction and the beam will catastrophically self-focus and eventually collapse. The critical peak power is of

several MW for standard optical glasses with large gap (e.g. silicate-based glasses; for fused silica $n_2 = 2.48 \times 10^{-16}\,\mathrm{cm}^2/\mathrm{W}$ [38]), but can decrease significantly for highly nonlinear glasses (e.g. chalcogenide types). The process is illustrated in Fig. 4(b). Due to self-focusing significant intensities can be in principle achieved at the collapse point. This catastrophic development can be arrested by the emergence of the carrier plasma, counteracting focusing effects. A way to overcome self-focusing is then to use tightly focused radiation, where material damage occurs before the achievement of the critical power for self-focusing. As apposed to self-focusing which depends on incident power, material damage is in this case a question of power density, where significant values can be achieved for relatively moderate input powers [39]. In parallel, the absorption acquires similarly a nonlinear character.

Plasma defocusing (PD): At the point of collapse, the intensity can be sufficiently high to ionize the material and to create an electron-hole plasma. In view of their light mass, the electrons will oscillate in the laser field and will thus develop as seen before a negative contribution to the real part of the refractive index. The spatial profile of the carrier density following nonlinearly the intensity distribution will create the equivalent of a negative lens, defocusing the incoming radiation. The effect becomes notable from relatively low electronic densities ($10^{17}\,\mathrm{cm}^{-3}$) and reduces effectively the focusing strength of the optics or arrests potential self-focusing. A certain self-control of excitation develops, which becomes robustly constant or even screened against the increase of input energy. This limits the quantity of energy that can be concentrated on the axis (intensity clamping), with energy spread outside the focal domain. When pulse self-focusing is balanced by plasma defocusing of the incoming light and standard diffraction, a filamentary propagation occurs [40,41], where the pulse propagates in a quasi-invariant way (Fig. 4(b)). Very short pulse ($< 100\,\mathrm{fs}$) will strongly promote filamentation at moderate focusing conditions. The effect is equally favored by a small reduced carrier mass. With a band structure that defines at low energies an effective electron mass (and thus in most cases in the presence of heavy holes a similar optical mass) smaller than the free electron mass [42] ($m_{eff} < m_e$), light scattering by carriers becomes effective.

Taking these processes into account, Fig. 4(c) gives an illustrative comparison between the energy distribution in the focal region of a short pulse in a linear and nonlinear regime. It is to be observed that the nonlinearity tends to spread and level out the energy distribution, depending on initial pulse width and focusing conditions. An experimental measurement of refractive index distribution is given in Fig. 4(d) (phase contrast microscopy image), showing a modulation of the index change corresponding to the fluence distribution.

Self-phase modulation (SPM): We have indicated above that the intensity dependence of the refractive index in a dielectric material has a spatial and a temporal component. The temporal equivalent of self-focusing (spatial) is the process of self-phase modulation. The time dependence of the refractive index

$n(t) = n_0 + n_2 I(t)$ will create a time dependent phase accumulation during light propagation inside the material $\Phi(t) = \frac{2\pi}{\lambda} n(t) L$, with L being the propagation distance. A time variation of the phase within the pulse will affect the spectral content. Thus, the pulse instantaneous frequency will vary as $\omega(t) = \partial\Phi(t)/\partial t$ and new spectral components are created (spectral broadening). In view of the propagation nonlinearity, this will influence the temporal envelope and the local light intensities. Spectacular phenomena such as continuum generation, pulse compression, or optical shocks can occur, with a strong spatio-temporal and spatio-spectral coupling.

Besides the spatio-temporal beam distortions, these phenomena lead to a transient variation of the refractive index, almost synchronous with the laser pulse or with short delayed dynamics, given by bound and free electrons. The real part contains thus contributions from the Kerr effect and from the free electron component.

$$\Delta n(t) = n_2 I(t) + \Re[\tilde{\Delta} n_{Drude}] \tag{5}$$

These are main contributions changing dynamically the dielectric function and thus the phase, acting in turn on the pulse itself (i.e. symmetric broadening for SPM and blue shifting for the plasma [43]). To this one can add contributions given by temperature (thermo-optic effect ($\Delta n(T)$) as well as transient density and pressure effects that are effective on timescales after the passage of the laser pulse. The final value of the index change will nevertheless rely on permanent material modifications generated by the energy deposition. Standard models of nonlinear propagation including the spatio-temporal distortions of the laser pulse can map in time and space the energy distribution [38,44,45], with current actions intending to derive material responses from first principles, coupled to the Maxwell's equations.

2.5 Matter relaxation

We have seen above that the process of ionization consists in the creation of an electron plasma where the relevant density for material processing can be between $10^{20}\,\mathrm{cm}^{-3}$ and $10^{22}\,\mathrm{cm}^{-3}$. At these densities the plasma rapidly can rapidly thermalize collisionally [31,46] and be defined by an electronic temperature T_e. We note that in between these values the plasma density can reach the so-called plasma resonance, where the plasma frequency $\omega_p = \sqrt{\rho_e e^2/\epsilon_0 m_e^*}$ equals the frequency of the driving light field. At this point the initial transparent material becomes strongly absorptive and reflective; a metal-like behavior, with its real dielectric function becoming zero. We note however that with a plasma damping time τ in the fs or sub-fs range this transition is not very abrupt and the plasma is dissipative. The energy transfer between light and plasma is maximized, and often the achievement of a critical density is used as a criterion for optical damage (which should be properly defined from energy balance considerations). This can be seen as a rather rough condition to signal that enough energy was deposited to promote phase transitions and

material modifications. In vacuum, the critical density of a free electron gas is $1.74 \times 10^{21}\,\mathrm{cm}^{-3}$. In a dielectric, the critical density is more difficult to be evaluated as the optical mass differs from the free electron mass in view of the band structure and hole coupling but the resonance condition takes the form $\omega_p = n_0\omega_{laser}$. It is interesting to evaluate the energy balance at this point. Considering also an average energy gain per electron comparable to the gap (lets say 10 eV), for these electron gas densities, a significant energy has been stored in the free electron system ($2700\,\mathrm{J/cm}^3$ for a density equal to the critical density in vacuum). In case of fused silica, this will lead to a temperature elevation of $\Delta T = E_{abs}/(c_p\rho_{glass})$. Considering the specific heat of fused silica $c_p = 0.74\,\mathrm{J/gK}$ and a density $\rho_{glass} = 2.2\ \mathrm{g/cm}^3$, the temperature augmentation is 1658 K, approaching the softening point $T_s = 1938\,\mathrm{K}$. This implies that low density promotes structural changes while higher densities trigger thermodynamic evolutions.

The plasma will relax, carriers will recombine (with a cascade of radiative and Auger processes) or give the excess energy to the matrix nonradiatively via vibrational activation and electron-phonon coupling or other forms of electron-matrix structural coupling. In other words, collisions between electrons and atoms will lead to atomic and molecular vibrations, where their incoherent character can be assimilated to heat (note that swift electronic excitation at low doses can first trigger charge displacements and coherent lattice vibration [47,48]). As the pulse duration is typically smaller than the characteristic time of electron-vibrational (phonon) transfer, material changes consuming the energy can appear before thermalization, limiting thus heat diffusion. The conditions are thus of non-equilibrium between electrons and phonons, both being characterized by different temperatures. The necessary condition is that the matrix energy gain is comparable to a transition energy. For strongly coupled material, molecular polarization effects can determine structural alterations and molecular displacements in the presence of trapped carriers. These latter changes do not require the definition of a temperature for the ions. As a rule of thumb, structural changes can be defined in the absence of temperature effects, can be driven by ionic temperature but not necessarily require el-phonon thermalization, or can occur in full equilibrium conditions. Depending on the level of energy, various processes can be discussed that can result in densification, rarefaction, or the formation of voids.

It is interesting for comprehension purposes to consider the case of a model glass, namely fused silica (a-SiO_2). The molecular structure of fused silica is based on a building block or structural unit of tetrahedral geometry with a central silicon Si atom surrounded in the four corners of the tetrahedron by oxygen O atoms. The O-Si-O bond is strong, determining a rather rigid structure. Fused silica is an interesting support for photonic applications but equally carries interest in opto-mechanical applications. This interest is largely based on a wide transparency, from ultraviolet down to near-infrared, low expansion coefficient, thermal, chemical and mechanical stability (all these changing with the potential presence of impurities or dopants; the thermomechanical and optical properties vary largely as a function of glass composition and con-

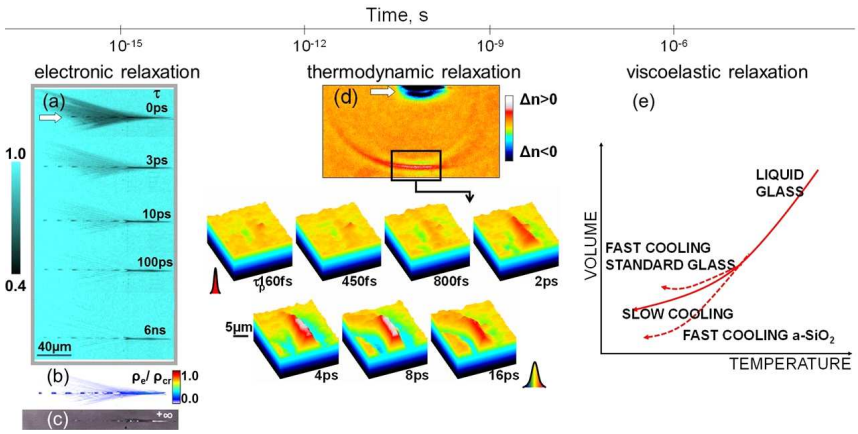

Fig. 5 Examples of relaxation processes with relevant timescales. (a) Electronic relaxation. Plasma decay via various channels with ultrafast or slow timescales as observed in time-resolved microscopy. (b) Estimation of the electronic density relative to the critical one. (c) Experimental detection of the final material transformation in terms of refractive index change (phase-contrast microscopy), indicating that fast relaxation is associated with low electron density levels, while slower relaxation channels can be associated with strong excitation. (d) Thermomechanical relaxation and emission of pressure waves. The magnitude of the pressure wave depends on the pulse duration. (e) Viscoelastic relaxation in glasses (standard and anomalous behavior) resulting in positive or negative density variations.

nectivity via the action of network formers and modifiers). The case of silicate glasses is nonetheless illustrative and a review of relevant relaxation processes in pure fused silica is given in Fig. 5 and contains electronic Fig. 5(a,b,c), thermomechanical (Fig. 5(d)) and viscoelastic relaxation processes (Fig. 5(e)). Let us first refer to the carrier relaxation (Fig. 5(a)) where a plasma is formed (evaluation of carrier density from transmission images is given in Fig. 5(b)), the energy of the electrons is transferred to the glass matrix, with the generation of a permanent index change (Fig. 5(c)). We discuss below the potential intermediate steps.

Carrier relaxation, bond breaking and defect formation: For relatively small carrier densities in the range of $10^{20}\,\mathrm{cm}^{-3}$, the matrix preserves the solid character and the excitation is only slightly perturbative to the band structure. The correlation between the electron and the hole leads to the formation of an exciton. The excitation weakly depletes the valence (VB) band that consists of bonding orbitals (dominantly mixed p oxygen orbitals) ensuring the cohesion of the glass matrix. The conduction band hosting the population of excited electrons contains antibonding states (s silicon states and a finite admixture of Si-O antibonding states [49]), indicating that the structural cohesion is less consistent. We therefore point out the first effect of electron excitation; the weakening of the molecular bonds. Secondly the free electrons can interact and polarize the matrix via a Coulomb potential in a rather strong manner. One effect in fused silica is therefore the trapping of the exciton (self-trapped

exciton STE). The exciton will be trapped by the self-induced polarization of the matrix and the associated deformation potential localizing charge on the orbitals. The process is rapid, on the order of 100 fs in view of the strong interaction between the electron and the matrix [50] (the case of slower relaxation for higher population levels will be discussed later on). This event will eventually break the Si-O bond. The impact is two-fold.

Defect formation: First, this leads to the generation of a defect or color center. The most common bond-breaking result is in the form of an oxygen dangling bond (NBOHC the non-bridging oxygen hole center) and a silicon dangling bond (E′ center). A rich literature exists on the topic [51]. The energy spectra associated with these defects consist of localized states in the forbidden energy gap, modifying thus both the real and the imaginary part dielectric function (connected via the Kramers-Kronig relations) and hence the refractive index. The energy diagram of defects corresponding to an index modification is given in Fig. 6(a). Such refractive index change is strongly dependent on the observation wavelength as it is based on a resonance with the defect levels: $\Delta n_{deff} \sim \sum \rho_{deff} f_{deff}/m(\omega_{deff}^2 - \omega^2)$, with f being the oscillator strength and ω_{deff}^2 being the defect resonance frequency (excitation frequency). This links the absorption spectra of the induced defects to the refractive index change [50,52].

The associated index change can be cured by low temperature heat treatment (e.g. few hundreds K [53]). A typical photoluminescence spectrum is given in Fig. 6(b) indicating the presence of defects. These are easily detectable via optical photoluminescence techniques following resonant excitation of defects or via electron paramagnetic resonance. For the case of fused silica, the NBOHC is the most commonly defect observed via optical techniques in positive refractive index change domains [54,55]. In parallel to the defect formation, consequence of the broken bond, atomic displacement (particularly the dangling O atom) occurs, again reflected in the index change. The observation underlines a structural link between the generation of defects and the resulting index change. At high doses, the Si-O bond can be broken in such a way that oxygen can be liberated [55,56], and Si atoms can further clusterize [57,58]. Oxygen deficiency centers appear [55].

The process is not limited to oxides. For example homopolar rebonding after bond breaking represents a mechanism of index change in chalcogenide glasses [59,60].

Structural rearrangements: A different consequence of bond breaking is that the structure can rearrange in different geometrical arrangements by a delayed rebonding. Again, a pertinent example is fused silica, with its rather open structure and its potential polymorphism [61] generated via ionization. The first consequence of laser irradiation is that the molecular structure of fused silica which consists mostly of six Si-O member rings, once a link was broken, will favor the apparition of smaller rings of three and four members [62,63], which is equivalent to compaction; more material in the same volume

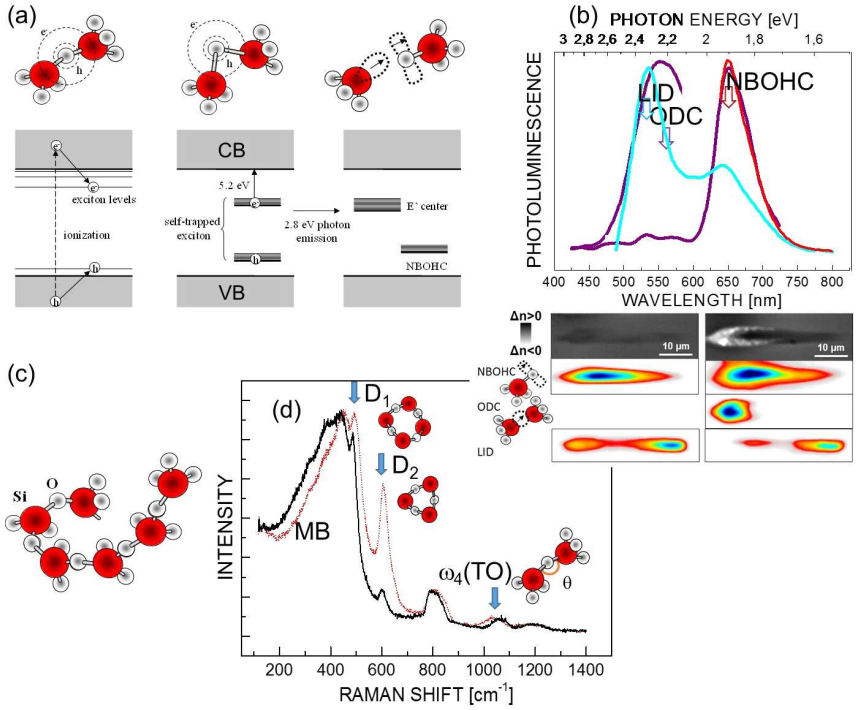

Fig. 6 Examples of relaxation processes. (a) The process of defect formation intermediated by exciton trapping in fused silica. (b). Typical photoluminescence spectra for ultrashort laser-induced positive refractive index changes. NBOHC are indicated together with other defect forms, related potentially to oxygen deficit. Refractive index image charts with their spatial photoluminescence map is given below (spectral signatures of NBOHC, ODC and types of unidentified laser-induced defects (LID)). (c) Schematic of structural reorganization following bond breaking. (d) Typical Raman spectrum for laser-induced positive index changes.

(Fig. 6(c)). This represents the so-called type I regime of positive index change, a terminology adopted from the field of Bragg gratings. An example of the corresponding Raman spectrum for the high index regime is given in Fig. 6(d), showing the variational features in the spectrum associated with structural rearrangements and compaction. Features corresponding to three and four member rings (D2 and D1) are augmented and the shift of spectral features signals compaction. We can state that in general in many optical glasses the generation of defects and bond breaking with structural rearrangements are correlated channels for refractive index changes. Each bond-breaking event will result in a dangling bond (defect) or in a rebonding process in potential smaller chains. Thus, the defect appearance will act as a marker of structural densification and index change.

Thermal relaxation: The collisional interaction of the electrons and the vibrational degrees of freedom (electron-phonon coupling) represent a generic

mechanism for heating the matrix. For strong-coupling materials (for example SiO_2) this interaction, strongly correlated to electronically-induced distortions is reflected in the high optical phonon energies (LO-phonon bands at 63 meV and 153 meV [42]), indicative of a potentially rapid heating mechanism.

Thermomechanical effects: If the carrier plasma density goes beyond the critical value, the energy stored in the electronic system can become significant. The electronic pressure augments to tens of GPa values, and, in the presence of a strong coupling mechanisms, ionic pressures can grow to values that exceed the mechanical strength of the solid. Shock and rarefaction occurs, with compressed material surrounding a core of rarefied matter (high-pressure phases may appear but marked by increased metastability [64]). Pressure release during the process can be visualized in Fig. 5(d), traveling as elastic waves at the speed of sound outside of the interaction region. The variation of density takes place, translating in a variation of the refractive index. High contrast low index zones may appear, down to a material fracture, denoted as type II (here strong excitation, potential decomposition and the appearance of interfaces show defects related to oxygen deficiency as seen in Fig. 6(b)). Along the energy transfer to the matrix, transitions towards liquid phases can occur or even the generation of dense plasma phase, the so-called warm dense matter. With the rise of temperature, a thermomechanical stress develops, with a local pressure drive being $P = \alpha_T Y \Delta T$ where α_T is the coefficient of thermal expansion and Y is the Young modulus. Depending on the strength of these values, thermal expansion and pressure release can become observable. Fused silica, being a low thermal expansion material ($\alpha_T = 5.5 \times 10^{-7}\,\mathrm{K}^{-1}$) with a rather rigid structure shows for example less thermal expansion effects as compared to a borosilicate glass (e.g. Schott BK7, a borosilicate crown optical glass) with approximately one order of magnitude higher coefficient. The result is a low index central core and even fracture due to rarefaction and a mechanically compressed high index surroundings where matter is preserved in a stress-compacted state, hence with a higher refractive index change. As a general rule, the presence of network modifiers can strongly modify the thermomechanical properties. Their presence in a silica matrix will loosen the strength of the covalent bonding creating less rigid bonds, and will favor expansion and rarefaction as the natural response to laser radiation.

Viscoelastic effects: If during the rise of the temperature low viscosity states are achievable, a process of structural reorganization occurs to accommodate the new thermodynamic equilibrium states. The speed of material restructuring to a new equilibrium structure is given by the ratio of the viscosity $\eta(T)$ and shear modulus $G(T)$, $\tau_{str} = \eta(T)/G(T)$. Depending on how close the temperature is with respect to the softening temperature, this time can vary over many orders of magnitude, dropping below microsecond for higher temperatures with respect to the softening temperature [65]. This can be easily understood considering a high molecular mobility in a hot low viscosity

matter. The temperature that reflects the newly obtained structural arrangement is the fictive temperature T_f. The variation of the fictive temperature is accompanied by a refractive index change [66]. It has to be noted here the singular behavior of fused silica with respect to other glass even silica-based. The anomalous behavior makes that silica will reduce its volume upon heating and fast cooling (high fictive temperature), while for a standard glass the response to heat is inverse (Fig. 5(e)). This again translates in refractive index variations. At the same time, at high temperatures a nucleation process can occur, forming gas bubbles into the glass.

We note here that these processes involving defect generation, bond reforming and structural rearrangements are generic and can be extended to other glasses [67]. However, the specific relaxation processes and their characteristic times may be different, as well as the thermodynamic behavior. With respect to the latter, fast cooling cycle generates higher density materials in fused silica, but in standard glasses the relaxation is accompanied by density decrease. Different relaxation time can be inferred as well, with longer relaxation times suggesting weakly coupling materials with a preponderance of thermal effects. An illustrative representation of different relaxation electronic times in fused silica and borosilicate BK7 is given in Fig. 7, where Fig. 7(a,b) describes electronic decay and onset of index change respectively. Two regions of interest emerge; a low carrier density region preceding the focal point and the focal region. It is interesting to note that in the low density areas preceding the focal region, the carrier decay is sub-ps in fused silica and few ps in BK7, while in the focal region the carrier lifetime seems significantly larger [68]. The fast electronic decay is accompanied by fast increase of the index in the low carrier density regions, and by a negative index change in the high carrier density regions. This suggests that the energy deposition is in this case sufficient to lead the discussion in terms of thermal transformations with heating, melting, shocking and rarefaction. On the side of a slow standard thermal evolution without mechanical waves, the evolution is driven by the thermodynamic nature of the glass. Fig. 7(c,d) indicate the results of a cooling cycle in standard glass and fused silica resulting, in view of the thermodynamic evolution, in density decrease respectively increase.

To conclude, several mechanisms concur to the refractive index change inside a transparent material. These mechanisms can be categorized as of electronic nature, structural nature and thermomechanical nature and they lead using the Clausius-Mossotti relation expressing the effect in the refractive index change to [69]:

$$\Delta n = \frac{(n^2+2)(n^2-1)}{6n}\left(\frac{\Delta\rho}{\rho}+\frac{\Delta R}{R}\right) \tag{6}$$

where $\Delta\rho/\rho$ expresses the relative change in density and $\Delta R/R = \Omega\Delta\rho/\rho$ is the relative change in the molar refractivity, related to the polarizability. Ω, the ratio of the relative polarizability change to the relative density change depends on the origin of modification and on the chemical composition, with values of Ω in the range -0.3 to -0.4 being reported [70]. The polarizability of

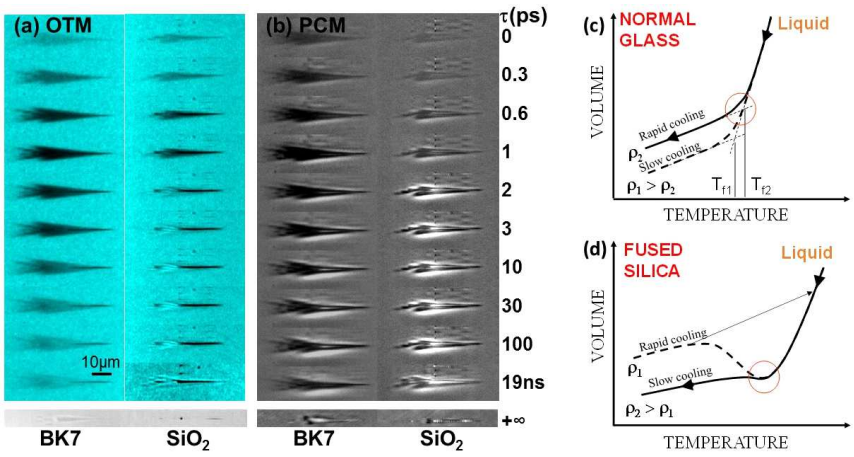

Fig. 7 Time-resolved observation of excitation and relaxation in borosilicate BK7 and fused silica in (a) optical transmission microscopy (OTM) and (b) phase-contrast microscopy (PCM) modes at energies moderately above the void-formation threshold. Input energy $E_D = 4\,\mu$J and pulse duration t_p=160 fs. Two characteristic regions in terms of dynamics are visible with fast and slow carrier decay times, and specific structural arrangements accompanying the two dynamics. The differentiation in fast and slow decay times is particularly observable for a-SiO_2, with a less pregnant distinction in the case of BK7.

the modified material has for optical frequencies mainly an electronic component related to the distortion of the electronic charge, being at the same time dependent on the laser-induced structural order, with structural and mechanical effects leading also to density variations. For example a change in the mean structural parameters of fused silica such as mean Si-O distance and mean Si-O-Si angle, or mean dihedral angle, should affect mean polarizability of the bound electrons. It similarly impacts the mean size of the member rings and affects the density, and spectroscopy data can help retrieving laser-induced index changes [71]. All these effects can be driven specifically using controlled irradiation. In crystals, amorphous domains can be formed with lower density and therefore low refractive index values [72].

Molecular and atomic element diffusion: If a heat source is formed, light dopant elements in glass will diffuse away following the temperature gradient, modifying locally the chemistry and the structure of the glass [73,74]. Acting as network modifiers, strong index changes can occur, depending on the mass and polarizability of the components [75]. In specific conditions molecular decomposition and phase separation occurs [65].

All the above-mentioned processes can be visualized in time in a dynamic way using pump probe techniques were the pump pulse induces the modification and the probe interrogates at specific delay times the irradiated region in evolution [76–78]. Dynamic studies have concentrated on the excitation and the evolution of the plasma, the electronic decay, trapping and recombination, but equally on the thermal and thermomechanical aspects [50,76–81].

The characteristic evolution time allows to determine to a certain extent the nature of the modification process. But moreover they will offer a guideline for optimizing the refractive index change.

3 Refractive index engineering

We have discussed above main mechanisms of refractive index change under ultrafast laser excitation, ranging from various modifications of the electronic bands, structural arrangements (electronic or heat-induced), or thermomechanical effects. At end effect, the amount of energy deposited in the solid and the rate of energy deposition will define the main interaction mechanisms and the magnitude or the sign of the refractive index changes.

Positive index changes for waveguides: In fused silica for example, ultrashort pulses favor soft positive (type I) index changes ($10^{-4} \div 10^{-3}$) as the filamentation will self-regulate the local intensity. The transformation relies mainly on defect-assisted densification following bond-breaking and generates isotropic index changes. This regime is then used for waveguide writing.

Negative index changes: With longer pulse envelopes or under tighter focusing conditions, the energy deposition may be sufficient to induce expansion, rarefaction and thermomechanical compaction. An example is given in Fig. 8(a,b), visualized as phase contrast images where dark colors indicate positive index changes and white color negative index changes or scattering. At high accumulation doses, a spectacular effect occurs, notably the spontaneous formation of an array of nanoscaled gratings [82] (Fig. 8(c) as a scanning electron microscopy image), i.e. a succession of empty and filled (high index) planes in the irradiated volume (the figure corresponds to a section of scanned traces fabricated in conditions similar to Fig. 8(b)). This is based on local interferences on laser-induced scattering centers, creating a periodicity of approximately $\lambda/2n$. The nanogratings bring anisotropy in the system and can be used for data storage, diffraction or color-marking of the solid [83]. At higher energy void regions can be obtained (type II, denomination used here for all low index regions). The quantity of deposited energy is equally important in other glasses. For example in borosilicate crown Schott BK7, the pulse duration can lead a transition between rarefaction and compaction (Fig. 8(d,e)) [84], controlling the stress fields in magnitude and geometry. These dependencies have led to smart irradiation techniques where the beam can be shaped in space and time to determine a user-defined response. Techniques for beam control will be discussed in a next section.

Many of the considerations discussed above are mostly pertinent for single pulse interactions and other factors may intervene for multipulse irradiation. At low laser repetition rates (kHz ranges), the effects will be exacerbated quasi-linearly with each incoming pulse before achieving an asymptotic level. As heat is not conserved in the interval between pulses, the effects will be

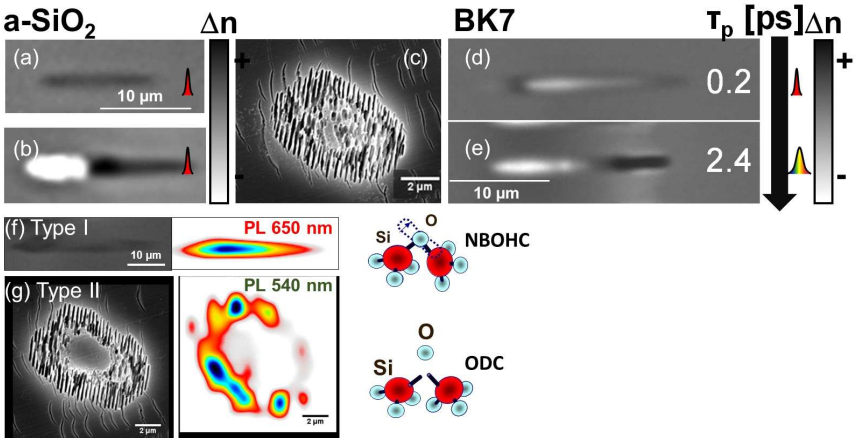

Fig. 8 (a,b) Examples of positive (type I) and negative (type II) index changes in fused silica [55]. These were obtained by acting on the pulse time envelope, dose and energy. Images are taken in phase contrast microscopy. Dark colors indicate positive index changes while white colors respectively negative index variations. (c) Nanoscale reorganization in fused silica (scanning electron microscopy picture). (d,e) Examples of laser-induced refractive index changes in borosilicate crown Schott BK7 [84]. (f,g) Morphology appearance correlated with spatially-resolved defects photoluminescence characteristic for type I and type II domains in fused silica (NBOHC and ODC respectively).

superposed on the existing trace by each of the incoming pulses, having in mind that with each defect creation, the absorption efficiency increases and the coupling of incoming pulses increases before saturation. Depending on the incident repetition rates we can discuss the following cases:

Incubation: The increase in the number of defects or structural units with the number of pulses (observed in photoluminescence studies and in the augmentation of Raman features, notably the D2 peak) is related to incubation. The association between defects and structural flaws enable at the same time chemical etching techniques that may enhance processing [85]. If for dielectrics incubation concerns mainly defect accumulation, other factors, notably mechanical may contribute (fatigue, accumulation of stress, etc.).

Heat accumulation: If the laser repetition rate augments to MHz (pulse interval comparable with the heat diffusion time), there is no longer time for the energy to diffuse away from the interaction region in the interval between two pulses. With each pulse, a heat accumulation process occurs, rising gradually the temperature to values that will locally melt and structurally change the solid, with enough time for a structural equilibration within the matrix corresponding to a higher temperature. The situation is graphically depicted in Fig. 9. The diffusion time is typically given by $t_{diff} \sim w^2/D$ with w being the dimension of the source and D the heat diffusion coefficient and goes typically on μs scales. The map of the refractive index change will depend on the ge-

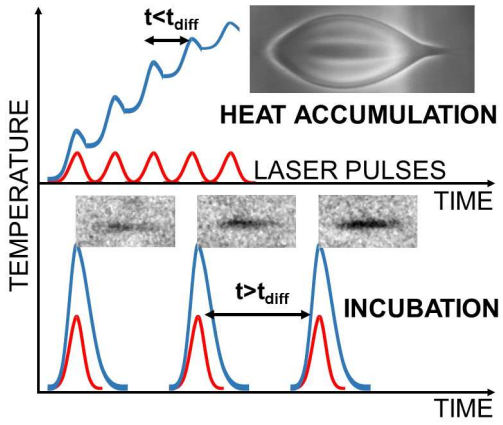

Fig. 9 Schematic description of incubative and heat accumulation regimes.

ometry of the heat source, with a size depending on the central temperature and sample diffusivity [86].

Stress waveguides: It was mentioned above that thermomechanical effects can generate stress-due compaction in the neighboring regions. Assembling together rarefaction traces in circular geometries can induce then a core of compacted material that can guide light, assisted equally by the depressed cladding from the rarefied regions [87], a mechanism supported by type II changes in glasses or by laser-induced amorphisation in crystalline dielectrics, where positive index increase is intrinsically difficult or metastable.

Other effects: Other refractive index changes are specifically related to the material nature and its characteristic interaction with light. These may be based on piezo-optic, pyroelectric, photo-refractive or photovoltaic effects where, for example, in the latter light-induced charge separation determines local polarization of matter. The above discussion can be extrapolated to various materials (from crystals to various glasses, silica based, heavy ion glasses, doped glasses or chalcogenide glasses). In spite of material specific properties, the phenomena presented above can be considered as generic events which offer a general frame of discussion.

3.1 Photoinscription strategies and control

3.1.1 Scan strategies

We have indicated above that the localized refractive index change is the building block for constructing optical functions. This can be achieved via replicating the index change in various 3D geometries by scanning the focused laser beam with respect to the sample. Several scan strategies were developed with

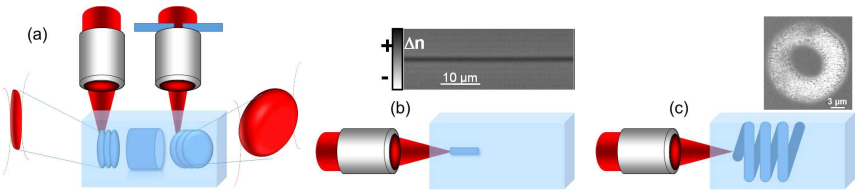

Fig. 10 Scan strategies for laser photoinscription. (a) Transverse scan. (b) Longitudinal scan. (c) Helicoidal scan and trepanning.

current scan speed in the mm/s range, matching the fabrication conditions for an industrial scale application of the process. A very first elementary function relates to the creation of a continuous scanned trace of positive refractive index change that can guide light. The achievement of this function implies linear displacement of the beam in the form of: transverse scan, perpendicular to the propagation direction, longitudinal scan, parallel to the propagation direction, helicoidal scan [3,4,55,88,89] (Fig. 10). The challenge is to create traces with symmetric sections on arbitrary geometries, rendering light transport insensitive to the polarization, and with a controllable and reproducible index change. The inherent difficulties come from (i) the elongated form of the confocal region, (ii) the emergence of spherical and chromatic aberrations, (iii) the size, and (iv) the material response. The solutions imply the design of the focal region and the control of the material response. Thus several focusing strategies were developed for transverse scan strategies to improve the symmetry of focusing. Astigmatic focusing and slit shaping expand the beam in one dimension creating a disk like focal region [90–92], being thus robust solutions to create symmetric waveguides. The slit can be virtually imprinted using spatial phase modulation, allowing a higher flexibility for creating bending and curved waveguides [93]. The symmetry will equally increase with the use of tight focusing and high repetition rates creating spherical heat-affected zones. These strategies can be equally used to improve index contrast (relying on incubation effects discussed earlier) and the spatial extent for the cross-section, in view of potential compatibility with larger wavelengths. In longitudinal scan strategies, the main limiting factor is related to spherical aberrations at the crossing of the air dielectric interface. The index mismatch elongates the confocal region with the focusing depth. The corrections imply compensating schemes in terms of energy and scan speed or the development of wavefront control. More complex spatial index distributions can be realized by trepanning or helicoidal scan involving longitudinal scan and helicoidal spin movement. This scan strategy creates a corona of index changes being optimal for depressed cladding or tubular design [88,89].

3.1.2 Advanced photoinscription control and optimality

The possibility to control the beam phase in a programmable way opens in addition extended means to control irradiation, and, at end effect, the result-

ing material modification [15,94]. This concept of beam engineering has been rendered feasible by the development of phase modulators either based on liquid- crystal technology, acousto-optic modulation or fast beam deflection (Fig. 11(a)) allowing equally to exert feedback and control in real times and in an automatic manner to the beam. All these technologies can change locally the phase (rotation of anisotropic liquid crystal molecules, diffraction on transient acoustic waves, etc.) and therefore can induce a modulation of the phase. A spatial modulation of the phase $\phi(r)$ or spectral modulation of the phase $\varphi(\omega)$ will correspond to a change in the spatial and temporal profile of the intensity at the focal point $I(r,t)$ (spatial and temporal pulse shaping). The different techniques are graphically summarized in Fig. 11. Often they can be accompanied by means of rapid monitoring of the interaction regions, allowing us to exert a real-time control on the photoinscription results in open and closed control loops. This refers to a situation where the irradiation results can be monitored in-situ (for example using amplitude and phase contrast optical imaging and interferometric methods) and the evaluation of the results allows to tune the spatial and temporal characteristics of the irradiation as to improve the processing result. Open loops define situations where a pre-established user control is exercised on the laser pulse, modifying predictively the spatial or temporal shapes, while closed loops presumes feedback presumably driven by an optimization algorithm. Several aspects of beam engineering are briefly discussed below, and for an in-depth presentation, the reader is referred to supplementary lectures. Let us first mention the spatial beam modulations as they are intuitive and straightforward:

Beam corrective effects: One of the main limitations of photoinscription is related to the position of the modification. The beam is prone to aberrations of the optical systems or to distortions during delivery. A main source of distortions is the spherical aberration. Whenever the focused, converging beam crosses the air/dielectric interface, the rays coming under various incidence angles will be refracted accordingly and will therefore converge on the axis on different positions (Fig. 11(b)). The effect will be exacerbated with even deeper focusing and by the use of higher numerical apertures. The standard correction techniques involve the use of collar corrected objectives, index matching liquids, or aspheric focusing elements. More recently, programmable spatial phase modulation was used correlated to the photoinscription scan to correct in a dynamic way for the depth-dependent aberrations [95,96] or other forms of spatial beam distortions. An example is given in Fig. 11(b), showing the corrective effect of the technique. Rapid corrections for correct beam delivery are key to a precise photoinscription process.

Parallel photoinscription: Spatial phase modulation techniques allows to multiply the foci and enable parallel processing techniques. In this case several focusing points can structure the material in the same time, being a time-effective processing solution. An example is given in (Fig. 11(c)), where several structures can be written in parallel. Given the programmable character of the

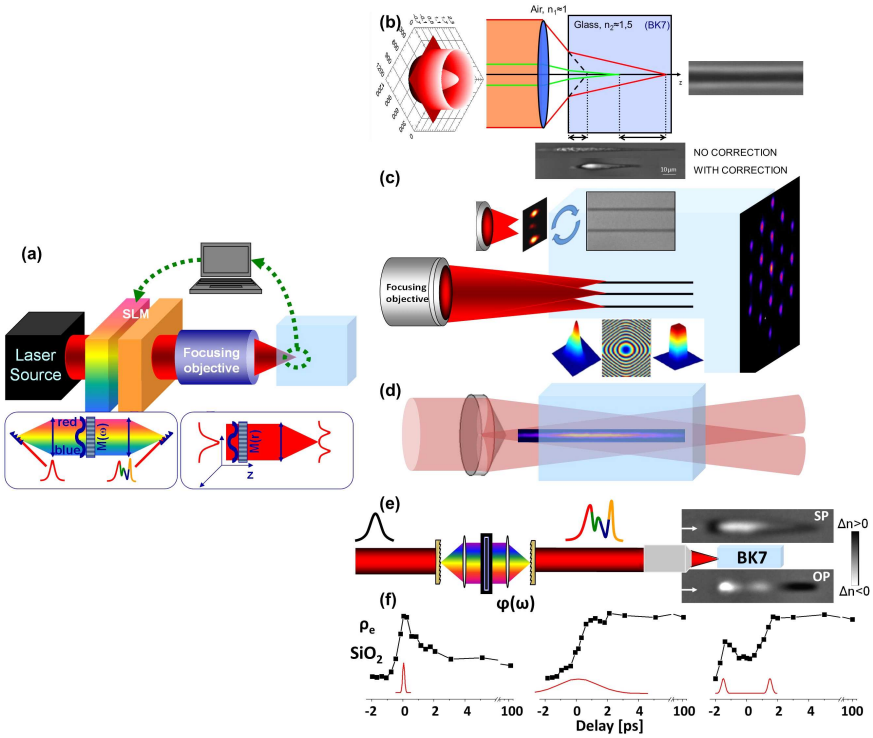

Fig. 11 (a) Smart scan strategies via spatio-temporal beam engineering. (b) Correction of aberrations [95]. (c) Parallel photoinscription [97]. (d) Non-diffractive structuring [22]. (e) Temporal pulse shaping [84] with index optimization in borosilicate BK7 glass. (f). Various dynamics of electronic populations (normalized) in fused silica induced by time-shaped pulses; short pulses, stretched pulses, double pulse sequences.

phase modulation, the pattern has a geometry that can vary during the scan, creating thus a flexible design. This procedure can significantly enhance the processing efficiency and decrease processing time, a constraint that should always be considered for industrial-scale applications [97–99].

Focal region shaping: In general the focal zone can be shaped to arbitrary forms [100], a feature of interest when considering the geometry of photoinscription (Fig. 11(c)). We only note here that the position of shaping may not correspond to the point of highest intensity and care should be taken to limit photoinscription only to the plane of spatial engineering. We also note new quasi 3D shaping techniques able to define the caustic of the beams and shape the full 3D space [101,102].

Non-diffractive irradiation: Recently applied to material processing [103,104], the non-diffractive Bessel beams put forward several advantages. Formed by conical intersection of wavefronts (convergence half angle θ and their constructive interference on the axis - for example the axicon lens imprints a conical

phase on an incoming plane phase of a Gaussian beam), these beams consist of a longitudinal pattern of light surrounded by regularly spaced rings (Fig. 11(d)). A zero-order Bessel beam is formed; $\mathcal{E}(t) = J_0(kr \sin\theta)$, with J_0 the zero-th order Bessel function of first kind, k the wavevector, and r the radial component. Prone to less nonlinear perturbation and quasi-free of spherical aberrations, these beams provide a strong confinement of energy.

Temporal beam shaping: We have seen above that the pulse temporal envelope critically depends on its bandwidth and on the relative spectral phase $\varphi(\omega)$. A user-defined change of the spectral phase permits the sculpting of the pulse in the temporal domain, as indicated in Fig. 11(d). This method of Fourier synthesis of frequencies has been facilitated by the above mentioned devices of optical modulation (acousto-optical or spatial light modulators) and several techniques were reviewed in [15] (see also the references therein). It is to be noted here that, for ultrashort pulses, optical modulation cannot be exercised directly in the time domain as no modulator can act with fs time dynamics, therefore the spectral phase modulation is the favored approach. The generation of spectrally modulated pulses using an SLM (spatial light modulator) is straightforward, requiring that the pulse is first dispersed spatially in frequency components using a grating. The collimated spectrally dispersed pulse encounters a liquid crystal array; the SLM. By controlling the rotation of the liquid crystal molecules at each position, the relative phase of the specific frequency can be altered. The pulse is then spectrally and spatially reformed by a second grating, preserving an imprinted temporal modulation. The resolution and the shaping window depend on the pulse bandwidth and the amount of frequency per pixel. Direct techniques of pulse synthesis with continuous phase control are based on acousto-optical dispersive filters [105] exploiting the interaction of timely-controlled acoustic waves with light.

The impact in material structuring is considerable from the viewpoint of a phenomenological effect [94] and laser processes can be globally optimized. It was indicated above that the relevant physical mechanisms of material transformations are driven by the amount of deposited energy and by the energy feedthrough rate. The mechanisms have equally different timescales of action; very rapid for electronic effects, slower for thermomechanical effects. Delivering energy on these relevant scale can emphasize specific channels of energy relaxation. This reflects the base of the concept of optimal control, i.e. the definition of irradiation sequences that can deliver, in this case, required forms of the refractive index change or in a general way processing efficiency. Coupling rapid monitoring with programmable modulation allows for the definition of iterative adaptive techniques for improving the result of laser structuring, driven by optimal search algorithms. These can work in a deterministic way (gradient methods, simplex methods) or non-deterministic, imitating biological evolution (genetic algorithms and evolutionary strategies). One of the first examples of applying adaptive temporal irradiation techniques for photoinscription is given in Ref. [84] suggesting how the heat source can be driven in size and shape to create a compacted material regions in borosilicate crown

glass BK7 using the generated stress fields. Orienting in space stress fields resulting from an intense heat source of particular shapes will generate extended regions of positive refractive index change. Examples of index design are given in Fig. 11(e). Equally, in fused silica shaped pulses can generate different dynamics of electronic relaxation [106] (see for example cases given in Fig. 11(e)) associated, as it will be shown later, with different morphological transformation (Fig. 11(f). As a general rule, the characteristic times of energy relaxation in glasses can be used as a guide line for control. Pulse bursts with repetition rates synchronized with electronic decay (i.e. THz rates) were advocated to create beneficial conditions for structuring of silica glasses [107]. Subtle effects induced by ps-scale pulse trains were found at the level of the microscopic structure, enhancing for example post-processing etching rates [108]. Changing the burst scale to MHz rates provides a different control knob, notably synchronization with thermal relaxation and softening; and a boost of processing efficiency [109,110].

A practical note is welcomed here. A precise shaping of the beam requires correlated phase and amplitude modulation, the latter being a source of energy loss. Therefore approximate solutions for beam engineering to well-defined patterns are necessary, that are able to match the required patter with high accuracy without generating additional losses (iterative Fourier algorithms). Recently, machine learning capacities were used for material structuring [111].

Spatio-temporal focusing: Often spatial and temporal effects are correlated via nonlinear effects and can generate mutual influences. Sometimes it is thus of interest to limit the region of high intensity below the size of the focal region. This can be obtained equally by spatially and spectrally dispersing and reforming the pulse. The geometry implies that during propagation the frequencies are not spatially overlapped (impeding the formation of a short pulse), but the process of pulse reforming and frequencies overlap will occur only upon focusing. This will limit the region of high intensity to narrower domains, without experience distortions during propagation [112,113]. Most of these techniques can be integrated in a single shaping device for increased processing flexibility [114].

The possibility to modulate the laser beam in space and time, with corresponding design of its vectorial character in synchronisation with the material carries the possibility to significantly upgrade the interaction in terms of quality, efficiency and processing scale.

3.2 Nanostructuring

Laser structuring implies the generation of a material function, e.g. in the optical domain. The processed function is critically dependent on the size of modification, originating in either individual or collective effects initiated by the structures. A specific interest exists in dimensional sizes significantly smaller that the optical wavelength. Notably in the optical domain, achieving

sub-100 nm structural sizes allows to access the electric field in embedded optical systems, sampling the oscillations. Collective optical effects (e.g. Bragg resonances) or field sampling effects can occur, reconstructing and manipulating the information within optical systems. However, this size is significantly smaller than the typical laser spot. We have seen before that due to diffraction the spatial dimension of irradiation through an optical system is limited to the diffraction limit, i.e. sub-μm. To bypass diffraction limits, the present irradiation strategies take advantage of nonlinear effects, evanescent field or beam engineering concepts that create strong confinement. The question of resolution is thus critical for industrial implementation of ultrafast lasers and the means to achieve the nanoscale optically is of importance [115]. First the nonlinear excitation [116] leads to a spatial confinement of radiation following a $I^N(r)$ law, as seen by the material. Avalanche effects induced by asymmetric pulse shapes can further amplify light confinement [117] only at the top of the intensity profile, adding a surplus of optical excitation on a limited region and demonstrating scales approaching 100 nm. The spot can be further downsized using approaches of focal spot engineering inspired from microscopy [118,119]. The emergence of a plasma in the dielectric and the onset of evanescent waves can further determine light concentration on scales significantly smaller than the wavelength [82]. To this we add the existence of a material threshold for processing, in the conditions where the laser creates itself the absorption centers [115]. Thus a highly reproducible material reaction is triggered by light, reaction which, in the presence of strong gradients, is no longer limited by the optical diffraction limit but by the material expansion at the speed of sound [120]. An example is the phenomenon of cavitation. Structures below 100 nm can thus be obtained. The process is equally effective at surfaces and in the bulk. We will discuss below two examples that combine light confinement and nanoscale structuring via cavitation.

Self-organization: Observed first by Shimotsuma et al. [82], regular sub-wavelength organization of matter in periodic patterns was the subject of numerous studies. Seen as part of a larger class of micron- and sub-micron-sized periodicities [122], they generate anisotropies, birefringence and polarization sensitivity. Several models based in plasma waves [82] or field-induced deformation of nanoplasmas [123] were proposed. A high-resolution study has pointed out the existence of gas-phase or decomposition nucleation centers developing in the nanoplanes [124]. Supported by this observation, electromagnetic models implying scattering on random microscopic centers and coherent superposition of wavelets were recently proposed [125,126]. The superposition leads to an interference process and a standing wave, patterning the excitation. Quasi-regular intensity maxima with evanescent components are generated, confining excitation. Whenever the material threshold is surpassed, in view of strong gradients, a planar fracture appears. The modified material changes in turn the scattering characteristics, generating a feedback process connecting light and the material in evolution. The emerging topographies will remodel scattering events in near and far-field, inducing, with each incoming pulse,

further order in the matter organization process at different periodicities and orientations. The light and the material exercise mutual influence. A synthesis illustrating this concept is indicated in Fig. 12 (a–c) with Fig. 12(a) proposing the conceptual model and its stages, Fig. 12(b) the experimental observation of nanogratings, and Fig. 12(c) modeling results of in-volume layered periodic electronic excitation. The typical periods and structural sizes can reach sub-100 nm values. It should be stressed that ultrashort pulses favor uniform type I regimes while the manipulation of time dose and energy generate birefringent nanostructured regions [121].

Direct focusing: Under strong NAs, the process of direct focusing can trigger high levels of excitation in confined regions, where stress relaxation determines the cavitation of the solid [127] and the generation of 100 nm structures. Whenever the energy density overcomes the cohesion energy of the material, a cavity occurs. The use of nondiffractive beams, with their strong confinement and nonlinear stability [128] can generate more tolerant conditions and achieve record nanostructuring sizes [103,104] in conditions of tight focusing or in combination with dispersion engineering. Fig. 12(d,e) show results of Bessel beam structuring on surfaces and in the bulk, with the possibility to obtain sub-100 nm structures.

As an example summarizing the discussion above and recalling different irradiation and relaxation concepts introduced here, we will briefly indicate below the transformation of fused silica from refractive index engineering to the achievement of nanoscale features via cavitation.

3.3 Multiscale dynamics

What is important to recall here is that the structuring process is driven by strong gradients. These gradients can be maximized in conditions of non-equilibrium. The essential role of ultrafast laser irradiation is to set these non-equilibrium conditions at the electronic, structural and thermodynamic level (pressure gradients and cooling rates). The interplay of different forms of laser generated non-equilibrium can confer a large flexibility to the light-matter interaction.

The example below discusses the interaction of an ultrafast Bessel-Gauss pulse with fused silica [76,129], recently reviewed in [130]. The utilisation of ultrashort pulses at moderate focusing geometries creates, as in the case of Gauss pulses, a positive index change that increases in magnitude with the number of pulses until reaching a saturation level in the 10^{-3} range. The main reason is related to a self-induced resistance of the material to damage, associated to the defocusing character of the electrons; the intensity clamping regime. Here the local intensity becomes self-regulated, all excess in energy being defocused away as to keep the balance between focusing and defocusing events. Being sensitive to the carrier densities, this interaction regime results therefore in relatively low electronic densities ($10^{19} - 10^{20}\,\mathrm{cm}^{-3}$), and

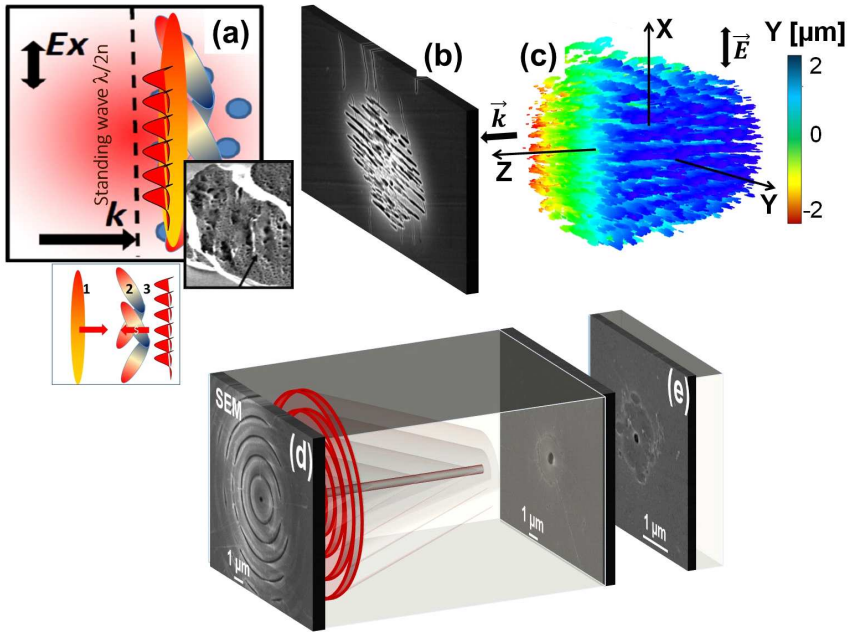

Fig. 12 (a) Coherent scattering and superposition concept with a blow-up of the irradiation steps: incident wavefront, scattered wavefront and interference pattern. The inset shows the presence of nanopores [124] (courtesy of M. Lancry) that serve presumably as scattering centers. (b) Nanogratings formed in bulk fused silica. (c) Electromagnetic modelling showing the regular patterns of electronic excitation. (d) Structuring surface and bulk with Bessel beams via direct focusing. (e) Sub-100 nm structures obtained by single-shot non-diffractive beam irradiation.

the solid is only slightly perturbed. The use of tighter focusing geometries or stretching the pulse in time will be able to overcome the energy loss due to carrier scattering and achieve high concentration of carrier densities (one order of magnitude higher) and energy concentrations sufficient to cavitate the material. The result of interaction is given in Fig. 13(a). The role of pulse stretching in maximizing energy deposition was also indicated for Gaussian pulses, as seen in Fig. 5(c). The carrier dynamics in type I conditions in fused silica shows the ultrafast carrier decay due to exciton self-trapping [50] with the raid onset of a high index material phase (Fig. 13(b,c,d)) from excitons and the presence of heat (insufficient though to induce enough heating as to determine a structural change [76]). The bond-breaking and the associated structural change results at the end in the generation of defects and structural densification (Fig. 13(e,f)). In type II condition, a higher concentration of energy is generated, sufficient presumably to generate a hot liquid phase quite fast. The carrier decay is much longer, indicating that the trapping strength in deformation potentials is significantly reduced, presumably due to a mix of electronic screening and vibrational (heat) effects. Upon the cooling phase, due to the stress, the void opens-up on hundreds of ns, consistent with a cavitation

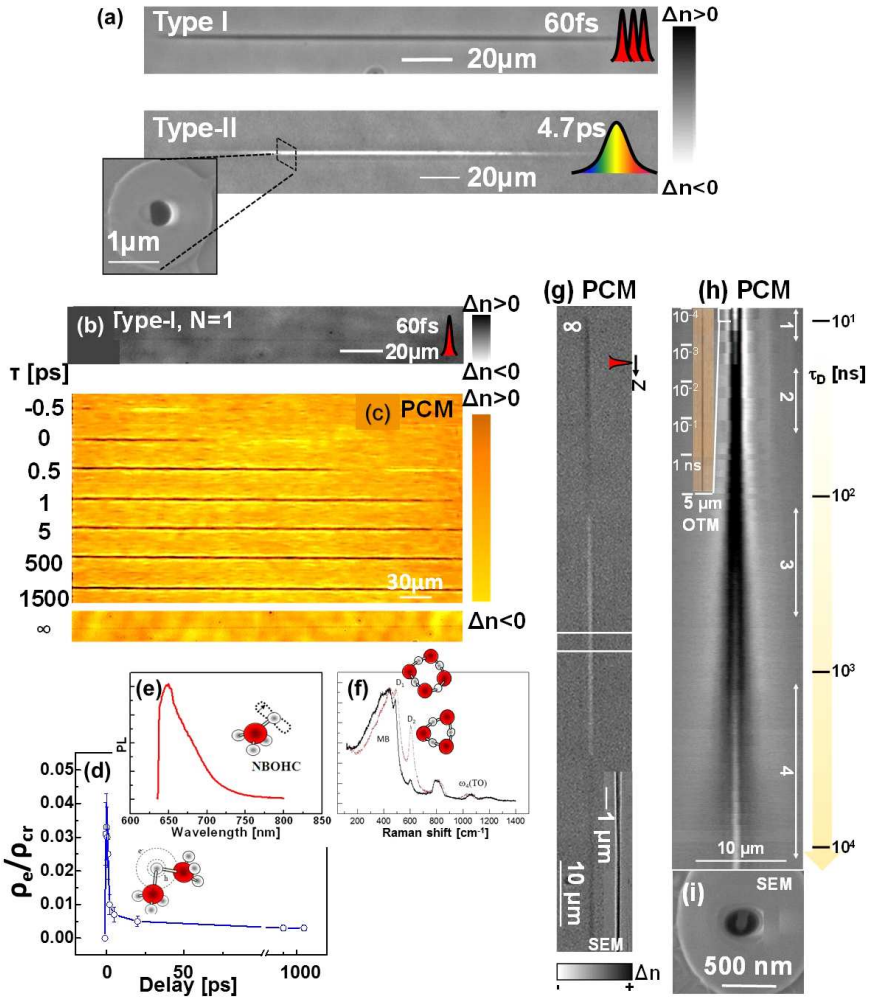

Fig. 13 (a) Type I positive index changes and type II void like structures induced in bulk fused silica by Bessel-Gauss beams with short (50 fs) and longer (4.7 ps) pulse duration (phase contrast microscopy). (b,c) Spatio-temporal ultrafast carrier dynamics in fused silica in type I conditions (b) showing the advance and rapid decay of the electron cloud (white light colors) and onset of a positive index change (dark colors) in the aftermath of the decay (c) [76]. (d) Electronic decay in time with ultrafast dynamics. (e,f) Photoluminescence and Raman spectra showing the presence of NBOHC and densified three-and four member rings after the rapid electronic relaxation. (g,h) Multiscale dynamics in type II conditions for the achievements of embedded voids. (g) Phase contrast microscopy image of low index structures. (h) Dynamic of modification over the entire relaxation cycle showing heating, heat diffusion and void opening on hundreds of ns timescale [129]. The inset indicates the long-living absorption associated with electrons. (i) A nanoscale void is formed.

process in the liquid phase [129]. The energetic balance indicates a transient regime between cavitation and gas-phase nucleation [130]. The size of the final void is on the few hundreds of nm and at low energies can go below 100 nm. A cavitation in the liquid phase is easier to achieve from a thermomechanical point of view than in a solid phase provided that heating occurs very fast, but solid cavitation and extreme conditions were reported in materials of high Young modulus [127]. These multiscale dynamic features illustrate the characteristic processes for forming index increase (defect-assisted densification) and void-like index decrease (thermomechanical processes) with access at the nanoscale.

4 Photonics applications

The possibility to engineer the refractive index in three dimensions can generate embedded optical functions, integrated in an optical chip [131–133], responding to present requirements of bandwidth and footprint. Besides the design flexibility, 3D concepts can be very effective in collection, transportation and manipulation of light via the refractive index magnitude and its space positioning (see for example [3]). A recent discussion, that will be briefly recalled here, was given in [16].

The elementary function is optical guiding in laser-written waveguides where refractive index engineering can define the propagation constant and modal characteristics. A significant effort was put in controlling losses, polarisation sensitivity or geometric flexibility with upgrades in scanning and positioning solutions, border roughness, beam delivery and material response. With the improvement of mechanical stability of workstations, as well of laser stability and irradiation control, optical losses can be found now in the range of 0.1-1 dBcm^{-1} for glasses and crystals, for standard (type I) and depressed clad waveguides respectively. Laser control can equally design the modal characteristics via the normalized frequency $V = \frac{2\pi a}{\lambda}\sqrt{(n+\Delta n)^2 - n^2}$ with a being the guide section. This parameter defines the single mode characteristics ($V < 2.4$) and the size of the mode with respect to the waveguide.

Starting with the waveguide block the refractive index change can be organized to perform some simple linear and nonlinear optical functions. Basic optical functions such as optical division, routing and splitting, evanescent coupling, directional or grating coupling, spectral filtering or modal control were generated, where the embedded character confers a significant phase stability [134–138]. Several of these functions are illustrated in Fig. 14(a), showing e.g. single mode guiding, splitting and large mode area guiding using evanescent coupling [97,139]. Optical division is one of the most important functions allowing to route light in optical circuits [134]. One of the mechanisms behind relies on evanescent coupling that, function of wavelength and distance, permits the evanescent component of the mode to penetrate in a adjacent waveguide situated in close-range, distributing light towards exit ports. This represents equally a solution for large mode area guiding using the syn-

chronous propagation in multicore waveguides and the achievement of super modes with large sections, particularly interesting for mid-infrared photonics [139]. Many photon starved applications require high collection efficiency using multimode collection and the transformation to single mode [140,141]. Here tapering or the concept of the photonic lantern [142] developed via laser photoinscription by Thomson et al. [141] are powerful concepts. In addition, filtering or multiplexing spectral components from a transmitted wavepacket may have interesting applications in optical communications. Realized by chromatic evanescent coupling or by modulations of the refractive index these types of functions have critical importance in optical telecommunications, laser development, and sensing. The periodic modulation of the refractive index creates a controllable spectral response, the Bragg resonance ($\lambda_B = 2n\Lambda/m$, with Λ the index periodicity and m the diffraction order). Via its sensitivity to mechanical and thermal dependencies of the refractive index, the Bragg grating waveguide [143,144] can be an efficient solution for optical communication, laser development and optical sensing, notably for temperature and stress fields. If the environment is nonlinear, the index, and therefore the propagation constant can be modulated by the mode intensity via the Kerr effect. The function becomes nonlinear. Examples can target various phenomena such as light localization, tuned nonlinearities, harmonic generation or saturable absorption [136,138,145,146]. Laser generation and amplification functions were demonstrated [147].

Assembling these functions, new fields of optical applications were generated, for example in: optical fabrication, telecom, analytics, optofluidics, optical storage, optomechanics, transport of quantum information, sensing, astrophotonics [83,148–153], relying essentially on the intrinsic mechanical stability of a laser-fabricated embedded chip. The backbone of telecommunication technology is based on guiding optics and new technologies are required to outcome limitations in bandwidth associated with single mode fibers and avoid capacity crunch [133]. 3D optical solutions were indicated; multicore fiber fan-out [154] and mode division multiplexers [155,156] including photonic lanterns [141,156], mode-selective directional couplers [157], mode-selective tapered velocity couplers [140] or multiplexers exploiting optical angular momentum [158], covering the entire telecommunication band in the 1500 nm range. Recent developments were indicated in [133]. Major progress was achieved in designing lab-on-chip devices that combine different functionalities on a single platform to transport, mix, separate and analyze biological samples in small volumes for the purpose of bio-chemical research, drug delivery or chemical synthesis. Most of these functions can be created by ultrashort pulses in potential combination with chemical methods etching the broken bonds in a monolithic glass or polymer substrate (and this is an essential feature in view of the required portability) and they can be classified as fluidic enabling functions or analytic functions [159,160]. In microfluidic devices laser-written waveguides can transport light at the point of analysis and recover light for the purpose of analysis (for example fluorescence or refractive index sensing).

We have seen that 3D optical design enables the manipulation of optical signals (filtering, amplification) in telecommunications, the connection of fluidic transport with optical probes in optofluidics, the permanent high capacity data storage using 3D laser modifications capabilities on the nanoscale and the associated birefringence, the coupling of optical and mechanical functions. In the latter cases, the capacity to create periodic nanostructures can increase the possibilities to encode information via birefringence and spatial modulation [83]. The mechanical expansion or compaction associated with material changes are susceptible to generate stress fields for controllable expansion and mechanically actuate system displacements [153].

Advances impact all fields of optics and relevant examples were given for optical sensing for chemical, thermal and mechanical fields, in transporting quantum information due to the intrinsic phase stability of an embedded optical chip, or in analytical sciences. A recent development field is related to remote detection, and, particularly a high demand for engineering optical functions in volume optical materials exists at the interface between optics and astronomy, notably for the fabrication of integrated astrophotonics instrumentation extending from planar to 3D geometries and providing photonic chip solutions [161,162]. The ultrafast laser photoinscription technique has enabled the inscription of novel 3D lightwave circuits, such as efficient multi-mode to single-mode converters for astronomical spectrographs as well as telescope pupil remappers and beam combiners for stellar interferometry. These are potential solutions to detect exoplanets, and miniaturized devices for on-sky detection were proposed. [150,163–165] Applications in astrophotonics were reviewed in several occasions ([140,161] and the reference therein), and will only briefly be recalled here. It is interesting to point out that commercial ultrafast laser solutions are already proposed for laser-fabricated integrated devices. Fabrication challenges still exist with respect to precise phase control, dispersion and chromatic management and polarization sensitivity, but the advantages are obvious. The accessibility to various spectral domains, notably the mid-infrared spectral range for photonics-based astronomical instruments is equally of importance in environmental sciences (for example detection of organic or CO_2 traces), putting forward the requirement of processing technologies for mid-infrared materials (e.g. chalcogenide glasses).

Using the achievements discussed above, we indicate below two examples of combined micro and nanostructures [166] creating a collective effect of optical resonances [167] and field sampling for accessing spectral information [168]. These examples require guiding solutions and field access and are represented in Fig. 14(b,c), indicating the upgrade in optical functions achieved by hybrid micro and nanostructures. The first example refers to a Bragg grating waveguide tuned on telecom wavelengths, where the light confinement capability of non-diffractive beams ensures a strong resonance [167]. The latter follows a powerful concept for spectrometry developed by Le Coarer et al. [169], where the field is read by nanoscatterers placed in the evanescent part of the mode [168]. These examples underline the importance of process control

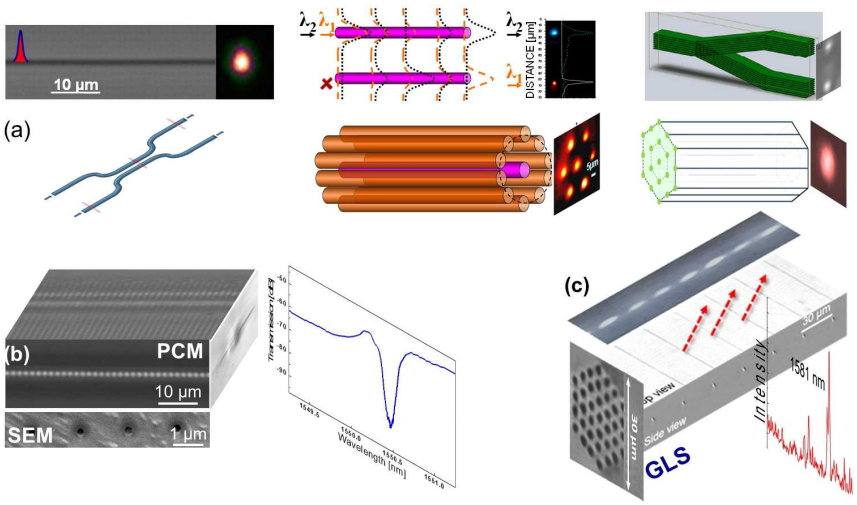

Fig. 14 (a) Basic laser-photoinscribed optical functions; single mode guiding, optical division, evanescent coupling, large-mode area guiding [16]. (b,c) Hybrid micro-nanoscale structures and optical functions. (b) Bragg gratings waveguide in fused silica at the 1500 nm telecom band where Bessel-induced nanostructures create a strong optical resonance [167]. (c) Field sampling in a chalcogenide GLS waveguide using Bessel-generated nanoscatterers diffracting and recreating the spectrum [168, 166].

on the smallest scales, intermediated by a complex but optimizable physics of interaction.

5 Conclusion and perspectives

The photonic chips are nowadays part of our society, enabling modern communication technology by transporting, multiplexing, converting and transforming information using light. Analogous to electronic circuits, the signal is transported by photon flux with information encoded in phase, amplitude, wavelength or polarization. Akin to harness all the characteristics of the photons, a new paradigm in optical conception is based on 3D designs [131]. Here the potential of focused ultrashort laser pulses comes into play, with an extraordinary flexibility in terms of substrate choice and processing parameters, with potential for mass production. Tens of research groups and several industrial players are now active in the field. Stressing the physical processes, this article only slightly uncovers the potential of 3D volume laser photoinscription which had an explosive development since the first demonstration of an ultrafast written waveguide in 1996, with extensions towards optical fabrication, telecom, microfluidics, and other fields of high-end optical applications.

We have briefly reviewed here the main concepts and mechanisms involved in the process of ultrafast laser photoinscription from both material and light sides. Using mainly fused silica as a model material, we have presented pho-

toinscription strategies and the emergence of spatio-temporal beam engineering techniques. These were conceived to steer nonlinearity in excitation and propagation and to deploy beam delivery corrections. The challenge is then to control a highly nonlinear process of excitation, where the matter transformation is intermediated by free carriers. A concept of optimality can be defined in the interaction process between light and matter, controlling the refractive index change or concurring to the achievement of the nanoscale. The structural modification can be regulated via the achieved electronic density from densification to rarefaction. The transient dynamics is then characteristic to the process and illustrates either rapid electronic interactions in the solid phase or thermomechanical effects. Several features are signatures of relaxation in the solid phase or are intermediated by the liquid phase. Applications in 3D photonics were indicated, where fabrication achievements demonstrate performances in terms of losses, design and spectral dependencies, that has already impacted the field of optical instrumentation, lasers, astronomy, biophotonics and sensing. Application fields in new technologies such as quantum optics and information are on their way [170]. In parallel, the capability to manipulate light in three-dimensional waveguides with controlled coupling can emulate electronic states and interaction potentials in solids, helping visualise quantum phenomena [171].

The perspectives are strongly related to the irradiation control and to the observation means. The recent progress in attosecond technology will permit to resolve non-equilibrium processes on the scale of the optical cycle, the electron redistribution on molecular orbitals, screening and collisional processes as well as band dynamics in the intense optical field [36,172]. The progress in nanostructuring [173] will require observation means with spatial resolution on the nm scale, making short wavelength sources, coherent or incoherent, independent or in combination with strong fields, a tool of choice. A short temporal duration will permit to observe nanostructuring processes in time at mesoscopic and microscopic scales, visualising both mass redistribution and structural changes. To these we add practical perspectives related to the significant development in laser sources in terms of tunable wavelengths and repetition rates. Control procedures based on artificial intelligence will interface then processes and tools. The ensemble of applications is manifold and covers standard domains such as optical fabrication, telecom or optofluidics, to newer potential in data storage and astrophotonics (see also [83,174,175]) as well as for non-conventional optics [176]. The newest tendencies harness the most recent developments in quantum optics and propose devices for quantum optical technologies and phase metrology [135,177]. This shows a significant openings towards new modern applications field with large potential for innovation.

Acknowledgements I am deeply grateful to all my colleagues, students, and collaborators that, over the years, massively contributed to the results reviewed here: A. Mermillod-Blondin, J. Bonse, A. Rosenfeld, I. V. Hertel, I. Burakov, N. M. Bulgakova, Yu. Meshcheryakov, C. Mauclair, C. D'Amico, J. P. Colombier, E. Silaeva, G. Cheng, G. Zhang, K.

Mishchik, P. K. Velpula, M. K. Bhuyan, M. Somayaji, M. Royon, J. Troles, G. Martin, S. Minardi, F. Courvosier, R. Antoine and many others. I thank them all.

Conflict of interest

The author declares that he has no conflict of interest.

References

1. H. Misawa and S. Juodkazis (eds.) 3D Laser Microfabrication: Principles and applications, (Wiley-VCH Chichester, 2006).
2. K. Sugioka and Y. Cheng, Ultrafast lasers – reliable tools for advanced materials processing, Light: Sci. Appl., 3, e149 (2014).
3. K. Itoh, W. Watanabe, S. Nolte and C. Schaffer, Ultrafast processes for bulk modification of transparent materials, MRS Bull., 31, 620–625 (2006).
4. K. M. Davis, K. Miura, N. Sugimoto, and K. Hirao, Writing waveguides in glass with a femtosecond laser, Opt. Lett., 21, 1729–1731 (1996).
5. E. N. Glezer and E. Mazur, Ultrafast-laser driven micro-explosions in transparent materials. Appl. Phys. Lett. 71, 882–884 (1997).
6. D. Ashkenasi, H. Varel, A. Rosenfeld, S. Henz, J. Herrmann, and E. E. B. Cambell, Application of self-focusing of ps laser pulses for three-dimensional microstructuring of transparent materials, Appl. Phys. Lett. 72, 1442–1444 (1998).
7. C. R. Giuliano, Laser-induced damage to dielectric materials. Appl. Phys. Lett. 5, 137–139 (1964).
8. R. W. Hopper and D. R. Uhlmann, Mechanism of Inclusion Damage in Laser Glass, J. Appl. Phys. 41, 4023 (1970).
9. D. W. Fradin and M. Bass, Comparison of laser-induced surface and bulk damage, Appl. Phys. Lett. 22, 157–159 (1973).
10. E. Yablonovitch and N. Bloembergen, Avalanche ionization and the limiting diameter of filaments induced by light pulses in transparent media. Phys. Rev. Lett. 29, 907–910 (1972).
11. A. Schmid, P. Kelly, and P. Bräunlich, Optical breakdown in alkali halides, Phys. Rev. B 16, 4569 (1977).
12. K. O. Hill, Y. Fujii, D. C. Johnson, and B. S. Kawasaki, Photosensitivity in optical fiber waveguides: Application to reflection filter fabrication. Appl. Phys. Lett. 32, 647–649 (1978).
13. C. G. Askins, T.-E. Tsai, G. M. Williams, M. A. Putnam, M. Bashkansky, and E. J. Friebele, Fiber Bragg reflectors prepared by a single excimer pulse, Opt. Lett. 17, 833–835 (1992).
14. D. von der Linde and H. Schüller, Breakdown threshold and plasma formation in femtosecond lasersolid interaction, J. Opt. Soc. Am. B 13, 216–222 (1996).
15. R. Stoian, M. Wollenhaupt, T. Baumert, and I.V. Hertel, Temporal pulse tailoring in ultrafast laser manufacturing technologies, in Laser Precision Microfabrication, Eds: K. Sugioka, M. Meunier, A. Piqué. (Springer Verlag, Heidelberg) 135, 121–144 (2010).
16. R. Stoian and C. Mauclair, Photoinscription par laser à impulsions ultrabrèves pour des systèmes optiques 3D, Tech. Eng. E6312 (2018).
17. M. Wollenhaupt, A. Assion, and T. Baumert, Femtosecond Laser Pulses: Linear Properties, Manipulation, Generation and Measurement. In Springer Handbook of Lasers and Optics, Ed. F. Trägger., 937-983 (Springer Science and Business Media 2007).
18. P. Balling and J. Schou, Femtosecond-laser ablation dynamics of dielectrics: basics and applications for thin films, Rep. Prog. Phys. 76 036502 (2013)
19. L. V. Keldysh, Ionization in the field of a strong electromagnetic wave. Soviet Physics JETP, 20, 1307–1314 (1965).
20. C. B. Schaffer, Interaction of femtosecond laser pulses with transparent materials, Ph. Thesis (Harvard University 2001).

21. W. Franz, Photon-Assisted Tunneling (Franz-Keldysh Effect), in Tunneling Phenomena in Solids 207–217 (Springer, 1969).
22. F. A. Buot, Zener effect, Wiley Encyclopedia of Electrical and Electronics Engineering, 1–32 (2014).
23. G. Orlando, C. R. McDonald, N. H. Protik, G. Vampa and T. Brabec, Tunnelling time, what does it mean? J. Phys. B: At. Mol. Opt. Phys. 47, 204002 (2014).
24. D.M. Simanovskii and H. A. Schwettman, Midinfrared optical breakdown in transparent dielectrics. Phys. Rev. Lett. 91, 107601 (2003).
25. A. P. Joglekar, H. Liu, G. J. Spooner, E. Meyhöfer, G. Mourou, and A. J. Hunt, A study of the deterministic character of optical damage by femtosecond laser pulses and applications to nanomachining. Appl. Phys. B: Las. Opt. 77, 2530 (2003).
26. B. C. Stuart, M. D. Feit, S. Herman, A. M. Rubenchik, B. W. Shore and M. D. Perry, Nanosecond-to-femtosecond laser-induced breakdown in dielectrics. Phys. Rev. B, 53, 1749–1761 (1996).
27. J. C. Miller (ed.) Laser ablation: Principles and Applications, Springer Series in Materials Science 26 (Springer Verlag, Berlin 1994).
28. B. Rethfeld, Unified Model for the Free-Electron Avalanche in Laser-Irradiated Dielectrics. Phys. Rev. Lett. 92, 187401 (2004).
29. R. Stoian, M. Boyle, A. Thoss, A. Rosenfeld, G. Korn, and I. V. Hertel, Dynamic temporal pulse shaping in advanced ultrafast laser material processing. Appl. Phys. A: Mater. Sci. Process. 77, 265-269 (2003).
30. D. Du, X. Liu, G. Korn and G. Mourou, Laser-induced breakdown by impact ionization in SiO_2 with pulse widths from 7 ns to 150 fs. Appl. Phys. Lett. 64, 3071–3073 (1994).
31. A. Kaiser, B. Rethfeld, M. Vicanek and G. Simon, Microscopic processes in dielectrics under irradiation by subpicosecond laser pulses. Phys. Rev. B, 61, 11437–11450 (2000).
32. A. Yamada and K. Yabana, Multiscale time-dependent density functional theory for a unified description of ultrafast dynamics: Pulsed light, electron, and lattice motions in crystalline solids. Phys. Rev. B 99, 245103 (2019).
33. A. Couairon an A. Mysyrowicz, Femtosecond filamentation in transparent media. Phys. Rep. 441, 47–189 (2007).
34. E. Abbe. H. Lawson, ed. Translated by Fripp HE. A contribution to the theory of the microscope and the nature of microscopic vision. Proceedings of the Bristol Naturalists' Society 1, 200–261 (London, UK: Williams & Northgate 1876).
35. R. W. Boyd, Nonlinear optics, (Academic Press 2007).
36. A. Sommer, E. M. Bothschafter, S. A. Sato, C. Jakubeit, T. Latka, O. Razskazovskaya, H. Fattahi, M. Jobst, W. Schweinberger, V. Shirvanyan, V. S. Yakovlev, R. Kienberger, K. Yabana, N. Karpowicz, M. Schultze and F. Krausz, Attosecond nonlinear polarization and lightmatter energy transfer in solids, Nature 534, 86–90 (2016).
37. J. H. Marburger, Self-focusing: theory. Prog. Quantum Electron. 4, 35–110 (1975).
38. I. M. Burakov, N. M. Bulgakova, R. Stoian, A. Mermillod-Blondin, E. Audouard, A. Rosenfeld, A. Husakou, and I. V. Hertel, Spatial distribution of refractive index variations induced in bulk fused silica by single ultrashort and short laser pulses. J. Appl. Phys. 101, 043506 (2007).
39. J. B. Ashcom, R. R. Gattass, C. B. Schaffer, and E. Mazur, Numerical aperture dependence of damage and supercontinuum generation from femtosecond laser pulses in bulk fused silica, J. Opt. Soc. Am. B 23, 2317–2322 (2006).
40. G. N. Steinberg, Filamentray tracks formed in transparent optical glass by laser beam self-focusing. I. Experimental investigation. Phys. Rev. A 4, 1182–1194 (1971).
41. M. M. T. Loy and Y. R. Shen, Small-scale filaments in liquids and tracks of moving foci, Phys. Rev. Lett. 22, 994–997 (1969).
42. D. Arnold, E. Cartier, D. J. DiMaria, Theory of high-field electron transport and impact ionization in silicon dioxide, Phys. Rev. B 49 10278–10297 (1994).
43. B. M. Penetrante, J. N. Bardsley, W. M. Wood, C. W. Siders, and M. C. Downer, Ionization-induced frequency shifts in intense femtosecond laser pulses. J. Opt. Soc. Am. B 9, 2032–2040 (1992).
44. J. Liao and J. R. Gulley, Timefrequency control of ultrafast plasma generation in dielectrics. J. Opt. Soc. Am. B 31, 2973–2980 (2014).

45. N. M. Bulgakova, V. P. Zhukov, Yu. P. Meshcheryakov, L. Gemini, J. Brajer, D. Rostohar, and T. Mocek, Pulsed laser modification of transparent dielectrics: what can be foreseen and predicted by numerical simulations? J. Opt. Soc. Am. B 31, C11–C14 (2014).
46. N. Brouwer and B. Rethfeld, Excitation and relaxation dynamics in dielectrics irradiated by an intense ultrashort laser pulse. J. Opt. Soc. Am. B 31, C28–C35 (2014).
47. K. von Volkmann, T. Kampfrath, M. Krenz, M. Wolf, and C. Frischkorn, Ultrafast dynamics of coherent optical phonons in α-quartz. Ultrafast Phenomena XVI, Springer Series in Chemical Physics, 92, p.235 (Springer-Verlag Berlin Heidelberg, 2009).
48. K. Sokolowski-Tinten, C. Blome, J. Blums, A. Cavalleri, C. Dietrich, A. Tarasevitch, I. Uschmann, E. Förster, M. Kammler, M Horn-von-Hoegen and D. von der Linde, Femtosecond X-ray measurement of coherent lattice vibrations near the Lindemann stability limit. Nature, 422 287–289 (2003).
49. K. L. Yip and W. B. Fowler, Electronic structure of SiO_2. II. Calculations and results. Phys. Rev. B 10, 14001408 (1974).
50. P. Martin, S. Guizard, P. Daguzan, G. Petite, P. D'Oliveira, P. Meynadier, and M. Perdrix, Sub-picosecond study of carrier trapping dynamics in wide-band-gap crystals. Phys. Rev. B, 55, 5799–5810 (1997).
51. L. Skuja, M. Hirano, H. Hosono, and K. Kajihara, Defects in oxide glasses. Phys. Stat. Sol. c 2, 15–24 (2005).
52. A. Gusarov, D. Doyle, A. Hermanne, F. Berhmans, M. Fruit, G. Ulbrich, and M. Blondel, Refractive-index changes caused by proton radiation in silicate optical glasses. Appl. Opt., 41, 678–684 (2002).
53. D. L. Griscom and E. J. Friebele, Fundamental radiation-induced defect centers in synthetic fused silicas: Atomic chlorine, delocalized E centers, and a triplet state. Phys. Rev. B 34, 7524–7533 (1986).
54. M. Watanabe, S. Juodkazis, H. Sun, S. Matsuo, and H. Misawa, Phys. Rev. B 60, 9959 (1999).
55. K. Mishchik, C. D'Amico, P. K. Velpula, C. Mauclair, A. Boukenter, Y. Ouerdane, and R. Stoian. Ultrafast laser induced electronic and structural modifications in bulk fused silica. J. Appl. Phys. 213 133502 (2013).
56. L. Bressel, D. de Ligny, E. G. Gamaly, A. V. Rode, and S. Juodkazis, Observation of O_2 inside voids formed in GeO_2 glass by tightly-focused fs-laser pulses. Opt. Mat. Express 1, 1150–1157 (2011).
57. K. Miura, K. Hirao, Y. Shimotsuma, M. Sakakura, and S. Kanehira, Formation of Si structure in glass with a femtosecond laser, Appl. Phys. A: Mat. Sci Process. 93, 183-188 (2008).
58. C. M. Pépin, E. Block, R. Gaal, J. Nillon, C. Hoenninger, P. Gillet, Y. Bellouard, Silicon formation in bulk silica through femtosecond laser engraving, ArXiv:1806.10802 (2018).
59. O. M. Efimov, L. B. Glebov, K. A. Richardson, E. Van Stryland, T. Cardinal, S. H. Park, M. Couzi, and J. L. Bruneel, Waveguide writing in chalcogenide glasses by a train of femtosecond laser pulses. Opt. Mater. 17, 379386 (2001).
60. A. Zoubir, M. Richardson, C. Rivero, A. Schulte, C. Lopez, K. Richardson, N. Ho, and R. Vallée, Direct femtosecond laser writing of waveguides in As_2S_3 thin films, Opt. Lett. 29, 748–750 (2004).
61. C. Fiori and R. A. B. Devine, Evidence for a wide continuum of polymorphs in a-SiO_2. Phys. Rev. B 33, 2972 (1986).
62. E. J. Friebele and P. L. Higby, Radiation effects in amorphous SiO_2 for windows and mirror substrates. In Laser induced dam- age in optical materials:1987, H. E. Banett, A. H. Guenther, D. Milam, B. E. Newman, M. Soileau (eds.), 89 (ASTM International, 1988).
63. J. Chan, T. Huser, S. Risbud, and D. Krol. Modification of the fused silica glass network associated with waveguide fabrication using femtosecond laser pulses. Appl. Phys. A: Mater. Sci. Process. 76, 367–372 (2003).
64. K. T. Park, K. Terakura, and Y. Matsui, Theoretical evidence for a new ultra-high-pressure phase in SiO_2, Nature, 336, 670 (1988).
65. M. Lancry, B. Poumellec, A. Chabid-Erraji, M. Beresena, and P. G. Kazansky, Dependence of the femtosecond laser refractive index change thresholds on the chemical composition of doped-silica glasses. Opt. Mat. Express, 1, 711–723 (2011).
66. R. Brückner, Properties and structure of vitreous silica. J. Non-Cryst. Solids, 5, 123–175 (1970).

67. K. Mishchik, A. Ferrer, A. Ruiz de la Cruz, A. Mermillod-Blondin, Y Ouerdane, A. Boukenter, J. Solis, and R. Stoian, Photoinscription domains for ultrafast laser writing of refractive index changes in BK7 borosilicate crown glass. Opt. Mat. Express 3, 67–85 (2013).
68. C. Mauclair, A. Mermillod-Blondin, K. Mishchik, J. Bonse, A. Rosenfeld, J. P. Colombier, and R. Stoian, Excitation and relaxation dynamics in ultrafast laser irradiated optical glasses. High-Power Laser Sci. Eng. 4, e46 (2016).
69. B. Poumellec, P. Niay, M. Douay, and J. F. Bayon, The UV-induced refractive index grating in Ge:SiO_2 preforms: additional CW experiments and the macroscopic origin of the change in index. J. Phys. D: Appl. Phys. 29, 1842-1856 (1996).
70. R.E. Schenker and W. G. Oldham. Ultraviolet-induced densification in fused silica. J. Appl. Phys. 82, 1065 (1997).
71. L. Bressel, D. de Ligny, C. Sonneville, V. Martinez, V. Mizeikis, R. Buividas, and S. Juodkazis, Femtosecond laser induced density changes in GeO_2 and SiO_2 glasses: fictive temperature effect. Opt. Mat. Express 1, 605–613 (2011).
72. T. Gorelik, M. Will, S. Nolte, A. Tünnermann, and G. Glatzel, Transmission electron microscopy studies of femtosecond laser induced modifications in quartz. Appl. Phys. A: Mater. Sci. Process., vol. 76, p. 309-311 (2003).
73. Y. Liu, M. Shimizu, B. Zhu, Y. Dai, B. Qian, J. Qiu, Y. Shimotsuma, K. Miura, and K. Hirao, Micromodification of element distribution in glass using femtosecond laser irradiation. Opt. Lett. 34, 136–138 (2009).
74. T. Toney-Fernandez, P. Haro-Gonzales, B. Sotillo, M. Hernandez, D. Jaque, P. Fernandez, C. Domingo, J. Siegel, and J. Solis. Ion migration assisted inscription of high refractive index contrast waveguides by femtosecond laser pulses in phosphate glass. Opt. Lett., 38, 5248–5251 (2013).
75. J. Siegel, J. M. Fernandez-Navarro, A. Garcia-Navarro, V. Diez-Blanco, O. Sanz, J. Solis, F. Vega, and J. Armengo, Waveguide structures in heavy metal oxide glass written with femtosecond laser pulses above the critical self-focusing threshold. Appl. Phys. Lett. 86, 121109 (2005).
76. P K. Velpula, M. K. Bhuyan, F. Courvoisier, H. Zhang, J. P. Colombier, and R. Stoian, Spatio-temporal dynamics in nondiffractive Bessel ultrafast laser nanoscale volume structuring. Laser Photonics Rev. 10, 230-244 (2016).
77. D. G. Papazoglou and S. Tzortzakis. In-line holography for the characterization of ultrafast laser filamentation in transparent media. Appl. Phys. Lett. 93, 041120 (2008).
78. Y. Hayasaki, M. Isaka, A. Takita, and S. Juodkazis, Time-resolved interferometry of femtosecond-laser-induced processes under tight focusing and close-to-optical breakdown inside borosilicate glass. Opt. Express, 19, 5725–5734 (2011).
79. K. Bergner, B. Seyfarth, K. A. Lammers, T. Ullsperger, S. Döring, M. Heinrich, M. Kumar, D. Flamm, A. Tünnermann, and S. Nolte, Spatio-temporal analysis of glass volume processing using ultrashort laser pulses. Appl. Opt. 57, 4618–4632 (2018).
80. B. Momgaudis, V. Kudriasov, M. Vengris, and A. Melninkaitis, Quantitative assessment of nonlinearly absorbed energy in fused silica via time-resolved digital holography. Opt. Express 27, 7699–7711 (2019).
81. M. Sakakura, M. Terazima, Y. Shimotsuma, K. Miura, and K. Hirao, Observation of pressure wave generated by focusing a femtosecond laser pulse inside a glass. Opt. Express 15, 5674–5686 (2007).
82. [Y. Shimotsuma, P. G. Kazansky, J. Qiu, and K. Hirao, Self-organized nanogratings in glass irradiated by ultrashort light pulses. Phys. Rev. Lett. 91, 247405 (2003).
83. J. Zhang, M. Gecevičius, M. Beresna, and P. G. Kazansky, Seemingly Unlimited Lifetime Data Storage in Nanostructured Glass. Phys. Rev. Lett. 112, 033901 (2014).
84. A. Mermillod-Blondin, I. M. Burakov, Yu. P. Meshcheryakov, N. M. Bulgakova, E. Audouard, A. Rosenfeld, A. Husakou, I. V. Hertel, and R. Stoian, Flipping the sign of refractive index changes in ultrafast and temporally shaped laser-irradiated borosilicate crown optical glass at high repetition rates. Phys. Rev. B, 77, 104205 (2008).
85. V. R. Bhardwaj, E. Simova, P. B. Corkum, D. M. Rayner, C. Hnatovsky, R. S. Taylor, B. Schreder, M. Kluge, and J. Zimmer, Femtosecond laser-induced refractive index modification in multicomponent glasses, J. Appl. Phys. 97, 083102 (2005).

86. S. M. Eaton, H. Zhang, P. R. Herman, F. Yoshino, L. Shah, J. Bovatsek, and A. Y. Aray, Heat accumulation effects in femtosecond laser written waveguides with variable repetition rate. Opt. Express, 13, 4708–4716 (2005).
87. F. Chen and J. R. Vazquez de Aldana, Optical waveguides in crystalline dielectric materials produced by femtosecond-laser micromachining, Laser Photonics Rev. 8, 251-275 (2014).
88. O. Caulier, D. Le Coq, V. Bychkov, and P. Masselin, Direct laser writing of buried waveguide in As_2S_3 glass using a helical sample translation. Opt. Lett., 38, 4213–4125 (2013).
89. A. Zoubir, C. Lopez, M. Richardson and K. Richardson. Femtosecond laser fabrication of tubular waveguides in poly(methyl methacrylate). Opt. Lett., 29, 1840–1842 (2004).
90. R. Osellame, S. Taccheo, M. Marangoni, R. Ramponi, P. Laporta, D. Polli, S. De Silvestri, and G. Cerullo, Femtosecond writing of active optical waveguides with astigmatically shaped beams. J. Opt. Soc. Am. B, vol. 20, no. 7, p. 1559-1567 (2003).
91. Y. Cheng, K. Sugioka, K. Midorikawa, M. Masuda, K. Toyoda, M. Kawachi and K. Shihoyama, Control of the cross-sectional shape of a hollow microchannel embedded in photostructurable glass by use of a femtosecond laser. Opt. Lett. 28, 55–57 (2003).
92. M. Ams, G. D. Marshall, D. J. Spence, M. J. Withford, Slit beam shaping method for femtosecond laser direct-write fabrication of symmetric waveguides in bulk glasses, Opt. Express 13, 5676–5681 (2005).
93. P. S. Salter, A. Jesacher, J. B. Spring, B. J. Metcalf, N. Thomas-Peter, R. D. Simmonds, N. K. Langford, I. A. Walmsley, and M. J. Booth, Adaptive slit beam shaping for direct laser written waveguides. Opt. Lett., 37, 470–472 (2012).
94. R. Stoian, Optimizing laser-induced refractive index changes in optical glasses via spatial and temporal adaptive beam engineering In Femtosecond Laser Machining, R. Osellame et al. Eds. Springer Topics in Applied Physics 123, p. 67-91 (Springer Verlag Berlin Heidelberg 2012).
95. C. Mauclair, A. Mermillod-Blondin, N. Huot, E. Audouard, and R. Stoian, Ultrafast laser writing of homogeneous longitudinal waveguides in glasses using dynamic wavefront correction. Opt. Express, 16, 5481–5492 (2008).
96. M. J. Booth, M. Schwertner, T. Wilson, M. Nakano, Y. Kawata, M. Nakabayashi, and S. Miyata, Predictive aberration correction for multilayer optical data storage. Appl. Phys. Lett. 88, 031109 (2006).
97. C. Mauclair, G. Cheng, N. Huot, E. Audouard, A. Rosenfeld, I. V. Hertel, and R. Stoian, Dynamic ultrafast laser beam spatial tailoring for parallel micromachining of photonic devices in bulk transparent materials. Opt. Express 17, 3531–3542 (2009).
98. S. Hasegawa and Y. Hayasaki, Adaptive optimization of a hologram in holographic femtosecond laser processing system. Opt. Lett. 34, 22–24 (2009).
99. M. Sakakura, T. Sawano, Y. Shimotsuma, K. Miura, and K. Hirao, Improved phase hologram design for generating symmetric light spots and its application for laser writing of waveguides. Opt. Lett. 36, 1065–1067 (2011).
100. N. Sanner, N. Huot, E. Audouard, C. Larat, J.-P. Huignard, and Brigitte Loiseaux, Programmable focal spot shaping of amplified femtosecond laser pulses, Opt. Lett. 30, 1479–1481 (2005).
101. J. A. Rodrigo, T. Alieva, E. Abramochkin, and I. Castro, Shaping of light beams along curves in three dimensions, Opt. Express 18, 20544–20555 (2013)
102. F. Courvoisier, R. Stoian, and A. Couairon, Ultrafast laser micro-and nano-processing with nondiffracting and curved beams. Opt. Las. Engineering Vol. 80, p. 125-137 (2016).
103. M. K. Bhuyan, F. Courvoisier, P. A. Lacourt, M. Jacquot, R. Salut, R. Furfaro, and J. M. Dudley, High aspect ratio nanochannel machining using single shot femtosecond Bessel beams. Appl. Phys. Lett. 97, 081102 (2010).
104. M. K. Bhuyan, P. K. Velpula, J. P. Colombier, T. Olivier, N. Faure, and R. Stoian, Single-shot high aspect ratio bulk nanostructuring of fused silica using chirp controlled ultrafast laser Bessel beams. Appl. Phys. Lett. 104, 021107 (2014).
105. P. Tournois, Acousto-optic programmable dispersive filter for adaptive compensation of group delay time dispersion in laser systems. Opt. Commun. 140 245–249 (1997).
106. C. Mauclair, Spatio-Temporal Ultrafast laser tailoring for bulk functionalization of transparent materials, PhD Thesis (Université Jean Monnet, St. Etienne, Freie Universität Berlin, 2010).

107. R. Stoian, M. Boyle, A. Thoss, A. Rosenfeld, G. Korn, I. V. Hertel, and E. E. B. Campbell, Laser ablation of dielectrics with temporally shaped femtosecond pulses. Appl. Phys. Lett. 80, 353–355 (2002).
108. M. Zhao, J. Hu, L. Jiang, K. Zhang, P. Liu and Y. Lu, Controllable high-throughput high-quality femtosecond laser-enhanced chemical etching by temporal pulse shaping based on electron density control. Sci. Rep. 5, 13202 (2015).
109. K. Mishchik, C. Javaux Leger, O. Dematteo Caulier, S. Skupin, B. Chimier, C. Hönninger, R. Kling, G. Duchateau, J. Lopez, Ultrashort pulse laser cutting of glass by controlled fracture propagation. J. Las. Micro. Nanoeng. 11, 66–70 (2016).
110. D. Esser, S. Rezaei, J. Li, P. R. Herman, and J. Gottmann, Time dynamics of burst-train filamentation assisted femtosecond laser machining in glasses. Opt. Express 19, 25632–25642 (2011).
111. B. Mills, D. J. Heath, J. A. Grant-Jacob, and R. W. Eason, Predictive capabilities for laser machining via a neuronal network. Opt. Express 26, 17245-17253 (2018).
112. J. Squier, J. Thomas, E. Bock, C. Durfee, and S. Backus, High average power Yb:CaF_2 femtosecond amplifier with integrated simultaneous spatial and temporal focusing for laser material processing. Appl. Phys. A: Mat. Sci. Process. 114, 209-214 (2014).
113. F. He, H. Xu, Y. Cheng, J. Ni, H. Xiong, Z. Xu, K. Sugioka, and K. Midorikawa, Fabrication of microfluidic channels with a circular cross section using spatiotemporally focused femtosecond laser pulses, Opt. Lett., 35, 1106–1108 (2010).
114. B. Sun, P. S. Salter, C. Roider, A. Jesacher, J. Strauss, J. Heberle, M. Schmidt, and M. J. Booth, Four-dimensional light shaping: manipulating ultrafast spatiotemporal foci in space and time. Light: Sci. Appl., 7, 17117 (2018).
115. A P. Joglekar, H. Liu, E. Meyhöfer, G. Mourou, and A. J. Hunt. Optics at critical intensity: Applications to nanomorphing. Proc. Nat. Acad. Sci. 101, 5856–5861 (2004).
116. Y. V. White, X. Li, Z. Sikorski, L. M. Davis, and W. Hofmeister. Single-pulse ultrafast-laser machining of high aspect nano-holes at the surface of SiO_2. Opt. Express 16, 14411–14420 (2008).
117. L. Englert, B. Rethfeld, L. Haag, M. Wollenhaupt, C. Sarpe-Tudoran, and T. Baumert. Control of ionization processes in high band gap materials via tailored femtosecond pulses. Opt. Express 15, 17855–17862 (2007).
118. F. Qin, K. Huang, J. Wu, J. Teng, C. W. Qiu, and M. Hong. A supercritical lens optical label-free microscopy: Sub-diffraction resolution and ultra-long working distance. Adv. Mater. 29, 1602721 (2017).
119. K. Mishchik, Y. Petit, E. Brasselet, A. Royon, T. Cardinal, and L. Canioni. Patterning linear and nonlinear optical properties of photosensitive glasses by femtosecond structured light. Opt. Lett. 40, 201–204 (2015).
120. D. E. Grady. The spall strength of condensed matter. J. Mech. Phys. Solids 1988, 36 353–384 (1988).
121. C. Hnatovsky, R. S. Taylor, P. P. Rajeev, E. Simova, V. R. Bhardwaj, D. M. Rayner, and P. B. Corkum, Pulse duration dependence of femtosecond-laser-fabricated nanogratings in fused silica. Appl. Phys. Lett. 87, 014104 (2005).
122. A. Rudenko, J.P. Colombier, S. Höhm, A. Rosenfeld, J. Krüger, J. Bonse, and T. E. Itina, Spontaneous periodic ordering on the surface and in the bulk of dielectrics irradiated by ultrafast laser: a shared electromagnetic origin. Sci. Rep. 7, 12306 (2017).
123. R. Taylor, H. Hnatovsky, and E. Simova, Applications of femtosecond laser induced self-organized planar nanocracks inside fused silica glass. Laser Photonics Rev. 2, 26–46 (2008).
124. M. Lancry, B. Poumellec, J. Canning, K. Cook, J. C. Poulin, and F. Brisset, Ultrafast nanoporous silica formation driven by femtosecond laser irradiation. Laser Photonics Rev. 7, 953–962 (2007).
125. R. Buschlinger, S. Nolte, and U. Peschel, Self-organized pattern formation in laser-induced multiphoton ionization. Phys. Rev. B 89, 184306 (2014).
126. A. Rudenko, J. P. Colombier, and T. E. Itina, From random inhomogeneities to periodic nanostructures induced in bulk silica by ultrashort laser. Phys. Rev. B 93, 075427 (2016).
127. S. Juodkazis, K. Nishimura, S. Tanaka, H. Misawa, E. G. Gamaly, B. Luther-Davies, L. Hallo, P. Nicolai, and V. T. Tikhonchuk. Laser-induced microexplosion in the bulk of a sapphire crystal: Evidence of Mb pressures. Phys. Rev. Lett. 96, 166101 (2006).

128. D. Faccio, E. Rubino, A. Lotti, A. Couairon, A. Dubietis, G. Tamošauskas, D. G. Papazoglou, and S. Tzortzakis, Phys. Rev. A 85, 033829 (2012).
129. M. K. Bhuyan, M. Somayaji, A. Mermillod-Blondin, F. Bourquard, J. P. Colombier, and R. Stoian. Ultrafast laser nanostructuring in bulk silica, a "slow" microexplosion. Optica 2017;4:951–958.
130. R. Stoian, M. K. Bhuyan, A. Rudenko, J. P. Colombier, and G. Cheng. High-resolution material structuring using ultrafast laser non-diffractive beams. Adv. Phys. X 4, 1659180 (2019).
131. S. Nolte, M. Will, J. Burghoff, and A. Tünnermann, Femtosecond waveguide writing: a new avenue to three-dimensional integrated optics, Appl. Phys. A: Mat. Sci. Process. 77, 109-111 (2003).
132. P. R. Herman, K. P. Chen, P. Corkum, A. Naumov, S. Ng, and J. Zhang, Advanced lasers for photonic device microfabrication. RIKEN Rev., 32, p. 31–35 (2001).
133. S. Gross and M. J. Withford, Ultrafast-laser-inscribed 3D integrated photonics: challenges and emerging applications. Nanophoton. 4, 332-352 (2015).
134. A. M. Streltsov and N. F. Borelli, Fabrication and analysis of a directional coupler written in glass by nanojoule femtosecond laser pulses. Opt. Lett. 26, 42–43 (2001).
135. L. Sansoni, F. Sciarrino, G. Vallone, P. Mataloni, A. Crespi, R. Ramponi, and R. Osellame, Polarization Entangled State Measurement on a Chip. Phys. Rev. Lett., 105, 200503 (2010).
136. A. Szameit, D. Blömer, J. Burghoff, T. Schreiber, T. Pertsch, S. Nolte, A Tünnermann, and F. Lederer, Discrete nonlinear localization in femtosecond laser written waveguides in fused silica. Opt. Express, 13, 10552-10557 (2005).
137. M. Thiel, G. Flachenecker, and W. Schade, Femtosecond laser writing of Bragg grating waveguide bundles in bulk glass. Opt. Lett. 40, 1266–1269 (2015).
138. S. Minardi, G. Cheng, C. DAmico, and R. Stoian, Low-power-threshold photonic saturable absorber in nonlinear chalcogenide glass. Opt. Lett., 40, 257–259 (2015).
139. R. Stoian, C. DAmico, M. Bhuyan, and G. Cheng, Ultrafast laser photoinscription of large-mode-area waveguiding structures in bulk dielectrics. J. Opt. Las. Tech. 80, 93 (2016).
140. S. Gross, N. Riesen, J. D. Love, and M. J. Withford, Three-dimensional ultra-broadband integrated tapered mode multiplexers. Laser Photonics Rev. vol. 8, no. 5, p. L81L85 (2014).
141. R. R. Thomson, T. A. Birks, S. G. Leon-Saval, A. K. Kar, and J. Bland-Hawthorn, Ultrafast laser inscription of an integrated photonic lantern. Opt. Express 19, 5698–5705 (2011).
142. D. Noordegraaf, P. M. W. Skovgaard, M. D. Nielsen, and J. Bland-Hawthorn. Efficient multi-mode to singlemode coupling in a photonic lantern. Opt. Express 17, 1988-1994 (2009).
143. A. Martinez, M. Dubov, I. Krushchev, and I. Bennion, Direct writing of fibre Bragg gratings by femtosecond laser. Electron. Lett.,vol. 40, p. 11701172 (2004).
144. G. D. Marshall, A. Ams, and M. Withford, Direct laser written waveguideBragg gratings in bulk fused silica. Opt. Lett., 31, 2690–2691 (2006).
145. D. Blömer, A. Szameit, F. Dreisow, T. Schreiber, S. Nolte, and A. Tünnermann, Nonlinear refractive index of fs-laser-written waveguides in fused silica. Opt. Express 14 (6), 2151-2157 (2006).
146. X. He, C. Fan, B. Poumellec, Q. Liu, H. Zeng, F. Brisset,G. Chen, X. Zhao, and M. Lancry, Size-controlled oriented crystallization in SiO_2-based glasses by femtosecond laser irradiation. J. Opt. Soc. Am. B 31, 376–381 (2014).
147. S. J. Beecher, R. R. Thomson, N. D. Psaila, Z. Sun, T. Hasan, A. G. Rozhin, A. C. Ferrari, and A. K. Kar, 320 fs pulse generation from an ultrafast laser inscribed waveguide laser mode-locked by a nanotube saturable absorber. Appl. Phys. Lett. 97, 111114 (2010).
148. W. Watanabe, D. Kuroda, K. Itoh, and J. Nishii, Fabrication of Fresnel zone plate embedded in silica glass by femtosecond laser pulses. Opt. Express vol. 10, no. 19, p. 978-983 (2002).
149. F. Sima, K. Sugioka, R. Martinez Vazquez, R. Osellame, L. Keleman, and P. Ormos, Three-dimensional femtosecond laser processing for lab-on-a-chip applications. Nanophoton. 7, 613–634 (2017).

150. N. Jovanovici, P. G. Tuthill, B. Norris, S. Gross, P. Stewart, N. Charles, S. Lacour, M. Ams, J. S. Lawrence, A. Lehman, C. Neil, J. G. Robertson, G. D. Marshall, M. Ireland, A. Fuerbach, and M. J. Withford, Starlight demonstration of the Dragonfly instrument: an integrated photonic pupil-remapping interferometer for high-contrast imaging. Monthly Notices of the Royal Astronomical Society, 427, 806-815 (2012).
151. R. Osellame, H. J. W. Hoekstra, G. Cerullo, and M. Pollnau, Femtosecond laser microstructuring: an enabling tool for optofluidic lab-on-chips. Laser Photonics Rev. 5, 442-463 (2011)
152. S. Juodkazis, M. Sudzius, V. Mizeikis, H. Misawa, E. G. Gamaly, Y. Liu, O. A. Louchev, and K. Kitamura, Three-dimensional recording by tightly focused femtosecond pulses in LiNbO3. Appl. Phys. Lett. 89, 062903 (2006).
153. Y. Bellouard, A. Champion, B. McMillen, S. Mukherjee, R. R. Thomson, C. Pépin, P. Gillet, and Y. Cheng, Stress-state manipulation in fused silica via femtosecond laser irradiation. Optica, vol. 3, 1285–1293 (2016).
154. R. R. Thomson, H. T. Bookey, N. D. Psaila, A. Fender, S. Campbell, S. Macpherson, J. S. Barton, D. T. Reid, and A. K. Kar, Ultrafast-laser inscription of a three dimensional fan-out device for multicore fiber coupling applications. Opt. Express, 15, 11691-11697 (2007).
155. P. Mitchell, G. Brown, R. R. Thomson, N. Psaila, and A. Kar - 57 Channel (19×3) spatial multiplexer fabricated using direct laser inscription. Optical Fiber Communications Conference and Exhibition (OFC), M3K.5 (2014).
156. B. Guan, B. Ercan, N. K. Fontaine, R. P. Scott, and S. J. B. Yoo, Mode-group-selective photonic lantern based on integrated 3D devices fabricated by ultrafast laser inscription. Optical Fiber Communications Conference and Exhibition (OFC), 1, W2A.16 (2015).
157. N. Riesen, S. Gross, J. D. Love, and M. J. Withford, Femtosecond direct-written integrated mode couplers. Opt. Express 22, 2985529861 (2014).
158. B. Guan, R. Scott, C. Qin, N. Fontaine, T. Su, C. Ferrari, M. Capuzzo, F. Klemens, B. Keller, M. Earnshaw, and S. J. B. Yoo, Free-space coherent optical communication with orbital angular, momentum multiplexing/ demultiplexing using a hybrid 3D photonic integrated circuit. Opt. Express 22, 145-156 (2014).
159. H. Sun, F. He, Z. Zhou, Y. Cheng, Z. Xu, K. Sugioka, and K. Midorikawa, Fabrication of microfluidic optical waveguides on glass chips with femtosecond laser pulses. Opt. Lett., 32, 1536-1548 (2007)
160. R. Martinez-Vazquez, R. Osellame, D. Nolli, C. Dongre, H. Van der Vlekkert, R. Ramponi, M. Pollnau, and G. Verullo, Integration of femtosecond laser written optical waveguides in a lab-on-chip. Lab Chip 9, 91–96 (2009).
161. J. Bland-Hawthorn and P. Kern, Astrophotonics: a new era for astronomical instruments. Opt. Express 17, 1880–1884 (2009).
162. R. R. Thomson, A. K. Kar, and J. Allington-Smith, Ultrafast laser inscription: an enabling technology for astrophotonics. Opt. Express 17, 1963–1969 (2009).
163. J. Tepper, L. Labadie, R. Diener, S. Minardi, J. U. Pott, R. R. Thomson Thomson, and S. Nolte, Integrated optics prototype beam combiner for long baseline interferometry in the L and M bands. Astron. Astrophys. 602, A66 (2017).
164. R. J. Harris, D. G. MacLachlan MACLACHLAN, D. Choudry, T. J. Morris, E. Gendron, A. G. Basden, G. Brown, J. R. Allington-Smith, and R. R. Thomson, Photonic spatial reformatting of stellar light for diffraction-limited spectroscopy. Mon. Not. Roy. Astron. Soc. 450, 428–434 (2015).
165. A. Saviuk, S. Minardi, F. Dreisow, S. Nolte, and T. Pertsch, 3D-integrated optics component for astronomical spectro-interferometry. Appl. Opt. 52, 4556–4565 (2013).
166. R. Stoian, M. K. Bhuyan, G. Cheng, G. Zhang, R. Meyer, and F. Courvoisier. Ultrafast Bessel beams; advanced tools for laser material processing. Adv. Opt. Technolog. 7, 165–174 (2018).
167. G. Zhang, G. Cheng, C. D'Amico, and R. Stoian. Efficient point-by-point Bragg gratings fabricated in embedded laser-written silica waveguides using ultrafast Bessel beams. Opt. Lett. 43, 2161–2164 (2018).
168. G. Martin, M. K. Bhuyan, J. Troles, C. DAmico, R. Stoian, and E. Le Coarer. Near infrared spectro-interferometer using femtosecond laser written GLS embedded waveguides and nano-scatterers. Opt. Express 25, 8386–8397 (2017).

169. E. Le Coarer, S. Blaize, P. Benech, I. Stefanon, A. Morand, G. Lerondel, G. Leblond, P. Kern, J. M. Fedeli, and P. Royer. Wavelength-scale stationary-wave integrated Fourier-transform spectrometry. Nat. Photonics 1, 473–478 (2007).
170. R. J. Chapman, M. Santandrea, Z. Huang, G. Corrielli, A. Crespi, M.-H. Yung, R. Osellame, and Alberto Peruzzo, Experimental perfect state transfer of an entangled photonic qubit, Nat. Commun. 7, 11339 (2016).
171. M. C. Rechtsman, J. M. Zeuner, Y. Plotnik, Y. Lumer, D. Podolsky, F. Dreisow, S. Nolte, M. Segev, and A. Szameit, Photonic Floquet topological insulators. Nature, 496, 196–200 (2013).
172. M. Lucchini, S. A. Sato, A. Ludwig, J. Herrmann, M. Volkov, L. Kasmi, Y. Shinohara, K. Yabana, L. Gallmann, and U. Keller, Attosecond dynamical Franz-Keldysh effect in polycrystalline diamond, Science 353, 916–919 (2016).
173. A. Ródenas, M. Gu, G. Corrielli, P. Paiè, S. John, A. K. Kar, and R. Osellame, Three-dimensional femtosecond laser nanolithography of crystals. Nat. Photonics 13, 105-109 (2019).
174. R. Osellame, G. Cerullo, and R. Ramponi (Eds) Femtosecond laser micromachining: photonic and microfluidic devices in transparent materials. (Springer, 2012).
175. K. Sugioka and Y. Cheng (Eds.) Ultrafast laser processing: from micro- to nanoscale. (Pan Stanford, 2013).
176. T. D. Gerke and R. Piestun, Aperiodic volume optics. Nat. Photonics 4, 188-193 (2010).
177. T. Meany, M. Gräfe, R. Heilmann, A. Perez-Leija, S. Gross, M. J. Steel, M. J. Withford, and A. Szameit, Laser written circuits for quantum photonics. Laser Photonics Rev. 9, 363-384 (2015).